Predictions of single field inflation for the tensor/scalar ratio and the running spectral index

Hector J. de Vega, Norma G. Sánchez

Predictions of single field inflation for the tensor/scalar ratio and the running spectral index

H. J. de Vega[1,2,*] and N. G. Sanchez[1,†]

[1]*Observatoire de Paris, LERMA, Laboratoire Associé au CNRS UMR 8112, 61, Avenue de l'Observatoire, 75014 Paris, France*
[2]*LPTHE, Laboratoire Associé au CNRS UMR 7589, Université Pierre et Marie Curie (Paris VI) et Denis Diderot (Paris VII), Tour 24, 5 ème. étage, 4, Place Jussieu, 75252 Paris, Cedex 05, France*

(Received 12 April 2006; published 21 September 2006)

We study the single field slow-roll inflation models that better agree with the available CMB and LSS data including the three years WMAP data: new inflation and hybrid inflation. We study these models as effective field theories in the Ginsburg-Landau context: a trinomial potential turns out to be a simple and well motivated model. The spectral index n_s of the adiabatic fluctuations, the ratio r of tensor to scalar fluctuations and the running index $dn_s/d\ln k$ are studied in detail. We derive explicit formulas for n_s, r and $dn_s/d\ln k$ and provide relevant plots. In new inflation, and for the chosen central value $n_s = 0.95$, we predict $0.03 < r < 0.04$ and $-0.000\,70 < dn_s/d\ln k < -0.000\,55$. In hybrid inflation, and for $n_s = 0.95$, we predict $r \simeq 0.2$ and $dn_s/d\ln k \simeq -0.001$. Interestingly enough, we find that in new inflation n_s is *bounded* from above by $n_{s\,\max} = 0.961\,528\ldots$ and that r is a *two* valued function of n_s in the interval $0.96 < n_s < n_{s\,\max}$. In the first branch we find $r < r_{\max} = 0.114\,769\ldots$. In hybrid inflation we find a critical value $\mu^2_{0\,\mathrm{crit}}$ for the mass parameter μ_0^2 of the field σ coupled to the inflaton. For $\mu_0^2 < \Lambda_0 M_{\mathrm{Pl}}^2/192$, where Λ_0 is the cosmological constant, hybrid inflation yields a blue tilted $n_s > 1$ behavior. Hybrid inflation for $\mu_0^2 > \Lambda_0 M_{\mathrm{Pl}}^2/192$ fulfills all the present CMB + LSS data for a large enough initial inflaton amplitude. Even if chaotic inflation predicts n_s values compatible with the data, chaotic inflation is disfavored since it predicts a too high value $r \simeq 0.27$ for the ratio of tensor to scalar fluctuations. The model which best agrees with the current data and which best prepares the way to the expected data $r \lesssim 0.1$, is the trinomial potential with negative mass term: new inflation.

DOI: 10.1103/PhysRevD.74.063519 PACS numbers: 98.80.Cq, 05.10.Cc, 11.10.−z, 98.70.Vc

I. INTRODUCTION AND RESULTS

Inflation was introduced to solve several outstanding problems of the standard Big Bang model [1] and became an important part of the standard cosmology. At the same time, it provides a natural mechanism for the generation of scalar density fluctuations that seed large scale structure, thus explaining the origin of the temperature anisotropies in the cosmic microwave background (CMB), as well as that of tensor perturbations (primordial gravitational waves) [2,3].

A distinct aspect of inflationary perturbations is that these are generated by quantum fluctuations of the scalar field(s) that drive inflation. After their wavelength becomes larger than the Hubble radius, these fluctuations are amplified and grow, becoming classical and decoupling from causal microphysical processes. Upon re-entering the horizon, during the matter era, these classical perturbations seed the inhomogeneities which generate structure upon gravitational collapse [2,3]. A great diversity of inflationary models predict fairly generic features: a Gaussian, nearly scale invariant spectrum of (mostly) adiabatic scalar and tensor primordial fluctuations, making the inflationary paradigm fairly robust. The Gaussian, adiabatic and nearly scale invariant spectrum of primordial fluctuations provide an excellent fit to the highly precise wealth of data provided by the Wilkinson Microwave Anisotropy Probe (WMAP) [4,5] Perhaps the most striking validation of inflation as a mechanism for generating *superhorizon* (''acausal'') fluctuations is the anticorrelation peak in the temperature-polarization (TE) angular power spectrum at $l \sim 150$ corresponding to superhorizon scales [4]. The confirmation of many of the robust predictions of inflation by current high precision observations places inflationary cosmology on solid grounds.

Amongst the wide variety of inflationary scenarios, single field slow-roll models provide an appealing, simple and fairly generic description of inflation. Its simplest implementation is based on a scalar field (the inflaton) whose homogeneous expectation value drives the dynamics of the scale factor, plus small quantum fluctuations. The inflaton potential is fairly flat during inflation. This flatness not only leads to a slowly varying Hubble parameter, hence ensuring a sufficient number of e-folds, but also provides an explanation for the Gaussianity of the fluctuations as well as for the (almost) scale invariance of their power spectrum. A flat potential precludes large nonlinearities in the dynamics of the *fluctuations* of the scalar field.

The current WMAP data seem to validate the simpler one-field slow-roll scenario [4,5]. Furthermore, because the potential is flat the scalar field is almost *massless*, and modes cross the horizon with an amplitude proportional to the Hubble parameter. This fact combined with a slowly varying Hubble parameter yields an almost scale invariant primordial power spectrum. The slow-roll approximation has been recently cast as a $1/N_{e\,\mathrm{folds}}$ expansion [6], where $N_{e\,\mathrm{folds}} \sim 50$ is the number of e-folds before

*Electronic address: devega@lpthe.jussieu.fr
†Electronic address: Norma.Sanchez@obspm.fr

the end of inflation when modes of cosmological relevance today first crossed the Hubble radius.

The observational progress permit to start to discriminate among different inflationary models, placing stringent constraints on them. The upper bound on the ratio r of tensor to scalar fluctuations obtained by WMAP [4,5] rules out the massless ϕ^4 model and *necessarily* implies the presence of a *mass term* in the inflaton potential [5,6].

Besides its simplicity, the trinomial potential is a physically well-motivated potential for inflation in the grounds of the Ginsburg-Landau approach to effective field theories (see, for example, Ref. [7]). This potential is rich enough to describe the physics of inflation and accurately reproduce the WMAP data [4,5].

The slow-roll expansion plus the WMAP data constraints the inflaton potential to have the form [6]

$$V(\phi) = N_{e\,\text{folds}} M^4 w(\chi), \tag{1.1}$$

where ϕ is the inflaton field, χ is a dimensionless, slowly varying field

$$\chi \equiv \frac{\phi}{\sqrt{N_{e\,\text{folds}}} M_{\text{Pl}}}, \tag{1.2}$$

$w(\chi) \sim \mathcal{O}(1)$ and M is the energy scale of inflation which is determined by the amplitude of the scalar adiabatic fluctuations [4] to be

$$M \sim 0.003\,19 M_{\text{Pl}} = 0.77 \times 10^{16}\ \text{GeV}.$$

Following the spirit of the Ginsburg-Landau theory of phase transitions, the simplest choice is a quartic trinomial for the inflaton potential [6,8]:

$$w(\chi) = w_0 \pm \frac{1}{2}\chi^2 + \frac{h}{3}\sqrt{\frac{y}{2}}\chi^3 + \frac{y}{32}\chi^4, \tag{1.3}$$

where the coefficients w_0, h and y are dimensionless and of order one and the signs $\pm$ correspond to large and small field inflation, respectively, (chaotic and new inflation, respectively). Inserting Eq. (1.3) in Eq. (1.1) yields,

$$V(\phi) = V_0 \pm \frac{m^2}{2}\phi^2 + \frac{mg}{3}\phi^3 + \frac{\lambda}{4}\phi^4, \tag{1.4}$$

where the mass m^2 and the couplings g and λ are given by the following see-saw-like relations,

$$\begin{aligned} m &= \frac{M^2}{M_{\text{Pl}}}, \qquad g = h\sqrt{\frac{y}{2N}}\left(\frac{M}{M_{\text{Pl}}}\right)^2, \\ \lambda &= \frac{y}{8N}\left(\frac{M}{M_{\text{Pl}}}\right)^4, \qquad V_0 = NM^4 w_0, \end{aligned} \tag{1.5}$$

where $N \equiv N_{e\,\text{folds}}$. Notice that $y \sim \mathcal{O}(1) \sim h$ guarantee that $g \sim \mathcal{O}(10^{-6})$ and $\lambda \sim \mathcal{O}(10^{-12})$ without any fine tuning as stressed in Ref. [6]. That is, the smallness of the couplings directly follow from the form of the inflaton potential Eq. (1.1) and the amplitude of the scalar fluctuations that fixes M [6].

The small coupling limit $y \to 0$ of Eqs. (1.3) and (1.4) corresponds to a quadratic potential while the strong coupling limit $y \to \infty$ yields the massless quartic potential. The extreme asymmetric limit $|h| \to \infty$ yields a massive model without quadratic term. In such limit the product $\tilde{M}^2 \equiv |h| M^2$ characterizes the energy scale of inflation and must be kept fixed since it is determined by the amplitude of the scalar fluctuations.

We study here new inflation with the trinomial potential Eqs. (1.3) and (1.4) and hybrid inflation (see below), the two models fulfill the observational constraints. We compute in both scenarios n_s, r and the running $dn_s/d\ln k$ as functions of the parameters of the models, derive explicit formulas for n_s, r and $dn_s/d\ln k$ and provide relevant plots. Moreover, we plot the ratio r and the running $dn_s/d\ln k$ as functions of the scalar index n_s. Since the value of n_s is now known [5,9–11], these plots allow us to *predict* the values of r and $dn_s/d\ln k$ for the different inflationary models considered. These predictions and plots are solely produced from theory and not from any fitting of the data.

The three years WMAP data indicate a red tilted spectrum ($n_s < 1$) with a small ratio $r < 0.28$ of tensor to scalar fluctuations [5]. The present data do not permit to find the precise values neither of the ratio r nor of the running index $dn_s/d\ln k$, only upper bounds are obtained [4,5]. We therefore think that the value of n_s [Eq. (4.2)] obtained through a fit of the data assuming $r = dn_s/d\ln k = 0$ is more precise than the values of n_s obtained through fits allowing both r and $dn_s/d\ln k$ to vary. Notice that $n_s = 0.95$ was independently found from the 2dF data under similar assumptions [9]. More precisely, from the three years WMAP data [5] as well as Ref. [9] we choose

$$n_s = 0.95 \pm 0.02. \tag{1.6}$$

This value is obtained with the priors $r = 0$ and $dn_s/d\ln k = 0$ [5].

We find that for $n_s = 0.95$ and any value of the asymmetry h [see Figs. 4 and 5], new inflation with the trinomial potential Eqs. (1.3) and (1.4) predicts

$$\begin{aligned} &\text{trinomial potential new inflation for } n_s \\ &= 0.95\text{: } 0.03 < r < 0.04 \\ &\text{and} \quad -0.00070 < dn_s/d\ln k < -0.00055. \end{aligned}$$

We find for the lower value $n_s = 0.93$,

$$\begin{aligned} &\text{trinomial potential new inflation for } n_s \\ &= 0.93\text{: } 0.003 < r < 0.015 \\ &\text{and} \quad -0.0011 < dn_s/d\ln k < -0.00033. \end{aligned}$$

Moreover, in new inflation with the trinomial potential, we find that n_s is *bounded* from above by

$$\text{new inflation}: n_s < n_{s\,\text{maximum}} = 0.961\,528\ldots.$$

For $n_s = 0.961528\ldots$ we have in this model $r = 0.114\,769\ldots$ (see Figs. 4 and 6). Interestingly enough,

there exists *two* values (two branches) of r for one value of n_s in the interval $0.96 < n_s < 0.961\,528\ldots$ [see Fig. 4]. The value $r_{\max} = 0.114\,769\ldots$ is the maximum r in the first branch. The values $0.16 \geq r \geq 0.114\,769\ldots$ correspond to a second branch of r as a function of n_s in the interval $0.96 < n_s < 0.961\,528\ldots$. In the first branch we have

$$r_{\max} = 0.114\,769\ldots.$$

The absolute maximum value $r_{\text{abs max}} = 0.16$ belongs to the second branch and corresponds to the quadratic monomial potential obtained from Eq. (1.3) at $y = 0$.

These predicted values of the ratio r fulfill the three years WMAP bound including SDSS galaxy survey [5]

$$r < 0.28(95\%\,\text{CL}). \tag{1.7}$$

Moreover, one can see from fig. 14 in Ref. [5] that $r < 0.1(68\%\,\text{CL})$ from WMAP + SDSS.

Chaotic inflation with the trinomial potential Eq. (1.3) and (1.4) yields larger values of r than new inflation for a given value of n_s [8]. More precisely, for $n_s = 0.95$ we find $r = 0.27$ for the binomial potential [8] (the trinomial potential introduces very small changes).

Therefore, although the value for n_s [Eq. (1.6)] is compatible both with chaotic and new inflation, the WMAP bounds on r *clearly disfavor* chaotic inflation. New inflation easily fulfils the three years WMAP bounds on r and prepares the way for the expected data on the ratio of tensor/scalar fluctuations $r \lesssim 0.1$.

In the inflationary models of hybrid type, the inflaton is coupled to another scalar field σ_0 with mass term $-\mu_0^2 < 0$ through a potential of the type [12]

$$\begin{aligned} V_{\text{hyb}}(\phi, \sigma_0) &= \frac{m^2}{2}\phi^2 + \frac{g_0^2}{2}\phi^2\sigma_0^2 + \frac{\mu_0^4}{16\Lambda_0}\left(\sigma_0^2 - \frac{4\Lambda_0}{\mu_0^2}\right)^2 \\ &= \frac{m^2}{2}\phi^2 + \Lambda_0 + \frac{1}{2}(g_0^2\phi^2 - \mu_0^2)\sigma_0^2 \\ &\quad + \frac{\mu_0^4}{16\Lambda_0}\sigma_0^4, \end{aligned} \tag{1.8}$$

where $m^2 > 0$, $\Lambda_0 > 0$ plays the role of a cosmological constant and g_0^2 couples σ_0 with ϕ.

The initial conditions are chosen such that σ_0 and $\dot{\sigma}_0$ are very small (but not identically zero) and therefore inflation is driven by the cosmological constant Λ_0 plus the initial value of the inflaton $\phi(0)$. The inflaton field $\phi(t)$ decreases with time while the scale factor $a(t)$ grows exponentially with time. The field σ_0 has an effective classical mass square

$$m_\sigma^2 = g_0^2\phi^2 - \mu_0^2. \tag{1.9}$$

Since the inflaton field ϕ decreases with time, m_σ^2 becomes negative at some moment during inflation. At such moment, spinodal (tachyonic) instabilities appear and the field σ_0 starts to grow exponentially. Inflation stops when both fields ϕ and σ_0 are comparable with $\dot{\phi}$ and $\dot{\sigma}_0$ and close to their vacuum values.

We find that the time when the effective mass of the field σ_0 Eq. (1.9) becomes negative depends on the values of μ_0^2 and $g_0^2\phi^2(0)$. For low values of μ_0^2 the field σ_0 starts to grow close to the end of inflation. On the contrary, for higher values of μ_0^2 the field σ_0 starts to grow well before the end of inflation. This is explained by the fact that the scale of time variation of σ_0 goes as μ_0^{-1}. σ_0 evolves slowly for small μ_0 and fastly for large μ_0 [see Figs. 7–11].

Only at $\Lambda = 0$ hybrid inflation becomes chaotic inflation with the monomial potential $(m^2/2)\phi^2$. For any value of $\Lambda > 0$ even very small, the features of hybrid inflation remain.

We compute n_s, r and $dn_s/d\ln k$ for hybrid inflation as functions of the parameters in the potential Eq. (1.8) and the initial value of the inflaton field [see Figs. 12–23].

The results of our extended numerical investigation of hybrid inflation can be better expressed in terms of the dimensionless variables

$$\Lambda \equiv \frac{2\Lambda_0}{M^4 N_{e\text{ folds}}},$$

$$\hat{\chi} \equiv \frac{\phi}{\sqrt{N_{e\text{ folds}}\Lambda}M_{\text{Pl}}} \quad \text{and} \quad \hat{\mu}^2 \equiv \frac{\mu_0^2 M_{\text{Pl}}^2 N_{e\text{ folds}}}{2\Lambda_0}.$$

We depict in Figs. 12–23 the observables n_s, r and the running index $dn_s/d\ln k$ as functions of Λ and n_s. We present a complete picture for hybrid inflation covering *two* different, blue tilted and red tilted, regimes. We find that for all the observables, the shape of the curves depends crucially on the mass parameter $\hat{\mu}^2$ of the σ field and the (rescaled) initial amplitude $\hat{\chi}(0)$ of the inflaton field.

We find a blue tilted spectrum ($n_s > 1$) for $\hat{\mu}^2 < \hat{\mu}^2_{\text{crit}} \simeq 0.13$ while for $\hat{\mu}^2 > \hat{\mu}^2_{\text{crit}}$ we can have either $n_s > 1$ or $n_s < 1$ depending on the initial conditions: for $\hat{\chi}(0) > \hat{\chi}(0)_{\text{crit}}$ we have $n_s > 1$, and for $\hat{\chi}(0) < \hat{\chi}(0)_{\text{crit}}$ we have $n_s < 1$. The value of $\hat{\chi}(0)_{\text{crit}}$ grows with $\hat{\mu}^2$: for $\hat{\mu}^2 = 0.5$, we find $\hat{\chi}(0)_{\text{crit}} = 2.7$ and for $\hat{\mu}^2 = 1.7$, we find $\hat{\chi}(0)_{\text{crit}} = 5.8$.

We see that $n_s > 1$ happens when the cosmological constant Λ_0 is large enough compared with $\mu_0^2 M_{\text{Pl}}^2 N_{e\text{ folds}}$. More precisely, $\hat{\mu}^2 < \hat{\mu}^2_{\text{crit}}$ for $\Lambda_0 > 192\mu_0^2 M_{\text{Pl}}^2$ using $N_{e\text{ folds}} = 50$. That is, for $\Lambda_0 < 192\mu_0^2 M_{\text{Pl}}^2$ we have either red or blue tilted spectrum as explained above.

For large Λ, $n_s - 1$, r and $dn_s/d\ln k$ always tend asymptotically to zero whatever be $\hat{\mu}^2$ and $\hat{\chi}(0)$.

We see from our calculations that all blue tilted values of (n_s, r) in the domain $1 < n_s < 1.15$, $0 < r < 0.2$ can be realized by the hybrid inflation model Eq. (1.8). However, at the light of the three years WMAP data Ref. [5] the blue tilted regime in hybrid inflation $\mu^2 < \mu^2_{\text{crit}}$ is strongly disfavored.

The situation is totally different in the red tilted regime $\hat{\mu}^2 > \hat{\mu}^2_{\rm crit} \simeq 0.13$ in hybrid inflation. The possible values of (n_s, r) for such regime of hybrid inflation are in the upper-right quadrant as shown in Fig. 24.

Hybrid inflation in the red tilted regime $\mu^2 > \mu^2_{\rm crit}$ and $\hat{\chi}(0) < \hat{\chi}(0)_{\rm crit}$ fulfills the three years WMAP value for n_s [see Eq. (4.2)] as well as the bound on the ratio r [Eq. (4.3)]. We can read from Fig. 20 and 22 that

$$\mu^2 > \mu^2_{\rm crit} \text{ hybrid inflation: } 0.2 > r > 0.14 \quad \text{and}$$
$$-0.001 < dn_s/d\ln k < 0 \quad \text{for } 0.952 < n_s < 0.97.$$

Notice that hybrid inflation in the red tilted regime yields a too large ratio $r > 0.2$ for $n_s < 0.95$.

At the central value $n_s = 0.95$ both new and hybrid inflation are allowed. However, for $n_s < 0.95$ hybrid inflation is in trouble ($r > 0.2$) while for $n_s > 0.962$ new inflation is excluded.

The potential which best agree with the red tilted spectrum and which best prepares the way to the expected data (a small $r \lesssim 0.1$) is the trinomial potential Eqs. (1.3) and (1.4) with negative mass term, that is small field (new) inflation. Hybrid inflation with a trinomial potential can also reproduce the present data in the red tilted regime $\mu^2 > \mu^2_{\rm crit}$ and $\hat{\chi}(0) < \hat{\chi}(0)_{\rm crit}$.

All calculations presented in this paper stem from the inflaton potential in the slow-roll approximation (dominant order in $1/N \simeq 1/50$). They do not use observational data as input. The analytical formulas and plots provided in the paper allow to read directly the predicted values of r and $dn_s/d\ln k$ as functions of n_s. In order to make illustrative predictions, we take the value $n_s = 0.95 \pm 0.02$, as a judicious choice. The reader can see directly from the plots presented here our predictions for r and $dn_s/d\ln k$ for future observational values of n_s.

II. THE INFLATON POTENTIAL AND THE $1/N_{e\,\text{folds}}$ SLOW-ROLL EXPANSION

The description of cosmological inflation is based on an isotropic and homogeneous geometry, which assuming flat spatial sections is determined by the invariant distance

$$ds^2 = dt^2 - a^2(t)d\vec{x}^2. \tag{2.1}$$

The scale factor obeys the Friedman equation

$$\left[\frac{1}{a(t)}\frac{da}{dt}\right]^2 = \frac{\rho(t)}{3M^2_{\rm Pl}}, \tag{2.2}$$

where $M_{\rm Pl} = 1/\sqrt{8\pi G} = 2.4 \times 10^{18}$ GeV.

In single-field inflation the energy density is dominated by a homogeneous scalar *condensate*, the inflaton, whose dynamics is described by an *effective* Lagrangian

$$\mathcal{L} = a^3(t)\left[\frac{\dot{\phi}^2}{2} - \frac{(\nabla\phi)^2}{2a^2(t)} - V(\phi)\right]. \tag{2.3}$$

The inflaton potential $V(\phi)$ is a slowly varying function of ϕ in order to permit a slow-roll solution for the inflaton field $\phi(t)$.

We showed in Ref. [6] that combining the WMAP data with the slow-roll expansion yields an inflaton potential of the form

$$V(\phi) = NM^4 w(\chi), \tag{2.4}$$

where χ is a dimensionless, slowly varying field

$$\chi = \frac{\phi}{\sqrt{N}M_{\rm Pl}}, \tag{2.5}$$

$w(\chi) \sim \mathcal{O}(1)$, $N \sim 50$ is the number of efolds since the cosmologically relevant modes exited the horizon until the end of inflation and M is the energy scale of inflation

The dynamics of the rescaled field χ exhibits the slow time evolution in terms of the *stretched* dimensionless time variable,

$$\tau = \frac{tM^2}{M_{\rm Pl}\sqrt{N}}. \tag{2.6}$$

The rescaled variables χ and τ change slowly with time. A large change in the field amplitude ϕ results in a small change in the χ amplitude, a change in $\phi \sim M_{\rm Pl}$ results in a χ change $\sim 1/\sqrt{N}$. The form of the potential, Eq. (2.4) and the rescaled dimensionless inflaton field Eq. (2.5) and time variable τ make manifest the slow-roll expansion as a consistent systematic expansion in powers of $1/N$ [6].

The inflaton mass around the minimum is given by a see-saw formula

$$m = \frac{M^2}{M_{\rm Pl}} \sim 2.45 \times 10^{13} \text{ GeV}.$$

The Hubble parameter when the cosmologically relevant modes exit the horizon is given by

$$H = \sqrt{N} m \mathcal{H} \sim 1.0 \times 10^{14} \text{ GeV} = 4.1m,$$

where we used that $\mathcal{H} \sim 1$. As a result, $m \ll M$ and $H \ll M_{\rm Pl}$. A Ginsburg-Landau realization of the inflationary potential that fits the amplitude of the scalar fluctuations remarkably well, reveals that the Hubble parameter, the inflaton mass and nonlinear couplings are see-saw-like, namely, powers of the ratio $M/M_{\rm Pl}$ multiplied by further powers of $1/N$. Therefore, the smallness of the couplings is not a result of fine tuning but a *natural* consequence of the form of the potential and the validity of the effective field theory description and slow roll. The quantum expansion in loops is therefore a double expansion on $(H/M_{\rm Pl})^2$ and $1/N$. Notice that graviton corrections are also at least of order $(H/M_{\rm Pl})^2$ because the amplitude of tensor modes is of order $H/M_{\rm Pl}$. We showed that the form of the potential which fits the WMAP data and is consistent with slow roll Eqs. (2.4) and (2.5) implies the small values for the inflaton self-couplings [6].

The equations of motion in terms of the dimensionless rescaled field χ and the slow time variable τ take the form,

$$\mathcal{H}^2(\tau) = \frac{1}{3}\left[\frac{1}{2N}\left(\frac{d\chi}{d\tau}\right)^2 + w(\chi)\right], \qquad (2.7)$$
$$\frac{1}{N}\frac{d^2\chi}{d\tau^2} + 3\mathcal{H}\frac{d\chi}{d\tau} + w'(\chi) = 0.$$

The slow-roll approximation follows by neglecting the $\frac{1}{N}$ terms in Eqs. (2.7). Both $w(\chi)$ and $h(\tau)$ are of order N^0 for large N. Both equations make manifest the slow-roll expansion as an expansion in $1/N$.

The number of e-folds $N[\chi]$ since the field χ exits the horizon until the end of inflation (where χ takes the value $\chi_{\rm end}$) can be computed in close form from Eqs. (2.7) in the slow-roll approximation (neglecting $1/N$ corrections)

$$\frac{N[\chi]}{N} = -\int_{\chi}^{\chi_{\rm end}} \frac{w(\chi)}{w'(\chi)} d\chi \leq 1. \qquad (2.8)$$

The amplitude of adiabatic scalar perturbations is expressed as [3,4,6,13,14]

$$|\Delta^{(S)}_{k\,\rm ad}|^2 = \frac{N^2}{12\pi^2}\left(\frac{M}{M_{\rm Pl}}\right)^4 \frac{w^3(\chi)}{w'^2(\chi)}. \qquad (2.9)$$

The spectral index n_s, its running and the ratio of tensor to scalar fluctuations are expressed as

$$n_s - 1 = -\frac{3}{N}\left[\frac{w'(\chi)}{w(\chi)}\right]^2 + \frac{2}{N}\frac{w''(\chi)}{w(\chi)},$$
$$\frac{dn_s}{d\ln k} = -\frac{2}{N^2}\frac{w'(\chi)w'''(\chi)}{w^2(\chi)} - \frac{6}{N^2}\frac{[w'(\chi)]^4}{w^4(\chi)} + \frac{8}{N^2}\frac{[w'(\chi)]^2 w''(\chi)}{w^3(\chi)}, \qquad (2.10)$$
$$r = \frac{8}{N}\left[\frac{w'(\chi)}{w(\chi)}\right]^2.$$

In Eqs. (2.8), (2.9), and (2.10) the field χ is computed at horizon exiting. We choose $N[\chi] = N = 50$.

Since, $w(\chi)$ and $w'(\chi)$ are of order one, we find from Eq. (2.9)

$$\left(\frac{M}{M_{\rm Pl}}\right)^2 \sim \frac{2\sqrt{3}\pi}{N}|\Delta^{(S)}_{k\,\rm ad}| \simeq 1.02 \times 10^{-5}. \qquad (2.11)$$

where we used $N \simeq 50$ and the WMAP value for $|\Delta^{(S)}_{k\,\rm ad}| = (4.67 \pm 0.27) \times 10^{-5}$ [4]. This fixes the scale of inflation to be

$$M \simeq 3.19 \times 10^{-3} M_{\rm PL} \simeq 0.77 \times 10^{16}\ \text{GeV}.$$

This value pinpoints the scale of the potential during inflation to be at the GUT scale suggesting a deep connection between inflation and the physics at the GUT scale in cosmological space-time.

We see that $|n_s - 1|$ as well as the ratio r turn out to be of order $1/N_{e\ \rm folds}$. This nearly scale invariance is a natural property of inflation which is described by a quasi-de Sitter space-time geometry. This can be understood intuitively as follows: the geometry of the universe is scale invariant during de Sitter stage since the metric takes in conformal time the form

$$ds^2 = \frac{1}{(H\eta)^2}[(d\eta)^2 - (d\vec{x})^2].$$

Therefore, the primordial power generated is scale invariant except for the fact that inflation is not eternal and lasts for $N_{e\ \rm folds}$. Hence, the primordial spectrum is scale invariant up to $1/N_{e\ \rm folds}$ corrections. The values $n_s = 1$, $r = 0$ and $dn_s/d\ln k = 0$ correspond to a critical point as discussed in Ref. [6]. This a Gaussian fixed point around which the inflation model hovers in the renormalization group sense with an almost scale invariant spectrum of scalar fluctuations during the slow-roll stage.

The WMAP results favored single inflaton models and among them new and hybrid inflation emerge to be preferable than chaotic inflation [8].

We analyze in the subsequent sections new inflation and hybrid inflation in its simple physical realizations within the Ginzburg-Landau approach (the trinomial potential) [8].

III. SPECTRAL INDEX n_s, RATIO r AND RUNNING INDEX $\frac{dn_s}{d\ln k}$ FOR NEW INFLATION WITH THE TRINOMIAL POTENTIAL

We consider here the trinomial potential investigated in Ref. [8]

$$V(\phi) = V_0 - \frac{m^2}{2}\phi^2 + \frac{mg}{3}\phi^3 + \frac{\lambda}{4}\phi^4. \qquad (3.1)$$

where $m^2 > 0$ and g and λ are dimensionless couplings.

The corresponding dimensionless potential $w(\chi)$ takes the form

$$w(\chi) = -\frac{1}{2}\chi^2 + \frac{h}{3}\sqrt{\frac{y}{2}}\chi^3 + \frac{y}{32}\chi^4 + \frac{2}{y}F(h), \qquad (3.2)$$

where the quartic coupling y is dimensionless as well as the asymmetry parameter h. The couplings in Eq. (3.1) and (3.2) are related by

$$g = h\sqrt{\frac{y}{2N}}\left(\frac{M}{M_{\rm Pl}}\right)^2, \qquad \lambda = \frac{y}{8N}\left(\frac{M}{M_{\rm Pl}}\right)^4, \qquad (3.3)$$

and the constant $F(h)$ is related to V_0 by

$$\frac{2}{y}F(h) = \frac{V_0}{NM^4}.$$

The constant $F(h)$ ensures that $w(\chi_+) = w'(\chi_+) = 0$ at the absolute minimum $\chi = \chi_+ = (8/y)^{1/2}(\Delta + |h|)$ of the potential $w(\chi)$. Thus, inflation does not run eternally. $F(h)$ is given by

$$F(h) \equiv \frac{8}{3}h^4 + 4h^2 + 1 + \frac{8}{3}|h|\Delta^3, \qquad \Delta \equiv \sqrt{h^2+1}.$$

The parameter h reflects how asymmetric is the potential. Notice that $w(\chi)$ is invariant under the changes $\chi \to -\chi$, $h \to -h$. Hence, we can restrict ourselves to a given sign for h. Without loss of generality, we choose $h < 0$ and shall work with positive fields χ.

Notice that $y \sim \mathcal{O}(1) \sim h$ guarantee that $g \sim \mathcal{O}(10^{-6})$ and $\lambda \sim \mathcal{O}(10^{-12})$ without any fine tuning as stressed in Ref. [6].

New inflation is obtained by choosing the initial field χ in the interval $(0, \chi_+)$. The inflaton χ slowly rolls down the slope of the potential from its initial value until the absolute minimum of the potential χ_+.

Computing the number of e-folds from Eq. (2.8), we find the field χ at horizon crossing related to the parameters y and h. It is convenient to define the field variable z:

$$z \equiv \frac{y}{8}\chi^2.$$

We obtain by inserting Eq. (3.2) for $w(\chi)$ into Eq. (2.8) and setting $N[\chi] = N$,

$$\begin{aligned} y = {} & z - 2h^2 - 1 - 2|h|\Delta + \frac{4}{3}|h|(|h| + \Delta - \sqrt{z}) \\ & + \frac{16}{3}|h|(\Delta + |h|)\Delta^2 \log\left[\frac{1}{2}\left(1 + \frac{\sqrt{z} - |h|}{\Delta}\right)\right] \\ & - 2F(h)\log[\sqrt{z}(\Delta - |h|)]. \end{aligned} \tag{3.4}$$

z turns to be a monotonically decreasing function of y: z decreases from $z = z_+ = (\Delta + |h|)^2$ until $z = 0$ when y increases from $y = 0$ until $y = \infty$. When $\sqrt{z} \to \sqrt{z_+}$, y vanishes quadratically,

$$y \overset{z \to z_+}{=} 2(\sqrt{z} - \sqrt{z_+})^2 + \mathcal{O}([\sqrt{z} - \sqrt{z_+}]^3).$$

We obtain in analogous way from Eqs. (2.9) and (2.10) the spectral index, its running, the ratio r and the amplitude of adiabatic perturbations,

$$\begin{aligned} n_s = {} & 1 - 6\frac{y}{N}\frac{z(z + 2h\sqrt{z} - 1)^2}{[F(h) - 2z + \frac{8}{3}hz^{3/2} + z^2]^2} \\ & + \frac{y}{N}\frac{3z + 4h\sqrt{z} - 1}{F(h) - 2z + \frac{8}{3}hz^{3/2} + z^2}, \end{aligned} \tag{3.5}$$

$$\begin{aligned} \frac{dn_s}{d\ln k} = {} & -\frac{2}{N^2}\sqrt{z}y^2\frac{(z + 2h\sqrt{z} - 1)(h + \frac{3}{2}\sqrt{z})}{[F(h) - 2z + \frac{8}{3}hz^{3/2} + z^2]^2} \\ & - \frac{24}{N^2}y^2z^2\frac{(z + 2h\sqrt{z} - 1)^4}{[F(h) - 2z + \frac{8}{3}hz^{3/2} + z^2]^4} \\ & + \frac{8}{N^2}y^2z\frac{(3z + 4h\sqrt{z} - 1)(z + 2h\sqrt{z} - 1)^2}{[F(h) - 2z + \frac{8}{3}hz^{3/2} + z^2]^3}, \end{aligned} \tag{3.6}$$

$$r = 16\frac{y}{N}\frac{z(z + 2h\sqrt{z} - 1)^2}{[F(h) - 2z + \frac{8}{3}hz^{3/2} + z^2]^2}, \tag{3.7}$$

$$|\Delta^{(S)}_{k\,\mathrm{ad}}|^2 = \frac{N^2}{12\pi^2}\left(\frac{M}{M_{\mathrm{Pl}}}\right)^4\frac{[F(h) - 2z + \frac{8}{3}hz^{3/2} + z^2]^3}{y^2z(z + 2h\sqrt{z} - 1)^2}. \tag{3.8}$$

IV. PREDICTIONS FOR NEW INFLATION WITH THE TRINOMIAL POTENTIAL

We plot n_s, its running and r in Figs. 1–3 as functions of $\log y$ for various values of the asymmetry of the potential h, y being the dimensionless quartic coupling. Figures 4 and 5 depict r and the running $dn_s/d\ln k$ as functions of n_s for various values of the asymmetry h.

We see that generically $n_s < 1$ and $dn_s/d\ln k < 0$ for new inflation for all values of the couplings.

In new inflation we have the absolute upper bound

$$\text{new inflation}: \; r \le r_{\text{abs max}} = \frac{8}{N} = 0.16, \tag{4.1}$$

which is attained by the quadratic monomial potential obtained from Eq. (3.2) at $y = 0$. On the contrary, in chaotic inflation r is bounded as

$$\text{chaotic inflation} \;\; 0.16 = \frac{8}{N} < r < \frac{16}{N} = 0.32.$$

This bound holds for all values the asymmetry parameter h. The lower and upper bounds for r are saturated by the quadratic and quartic monomials, respectively.

We see from Fig. 1 that n_s exhibits a single maximum $n_{s\,\text{maximum}}(h)$ as a function of the quartic coupling y for

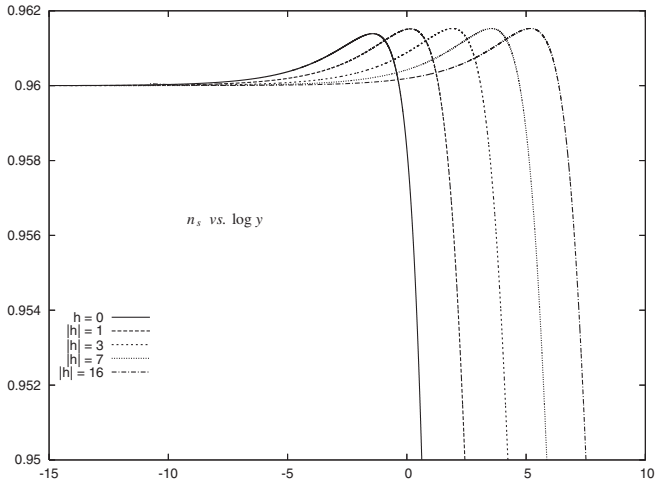

FIG. 1. New Inflation. n_s as a function of $\log y$ for the asymmetry of the potential $|h| = 0$, 1, 3, 7 and 16, y being the dimensionless quartic coupling. The $y \to 0$ limiting value $n_s = 1 - \frac{2}{N} = 0.96$ is h-independent and corresponds to the monomial potential $\frac{1}{2}m^2\phi^2$.

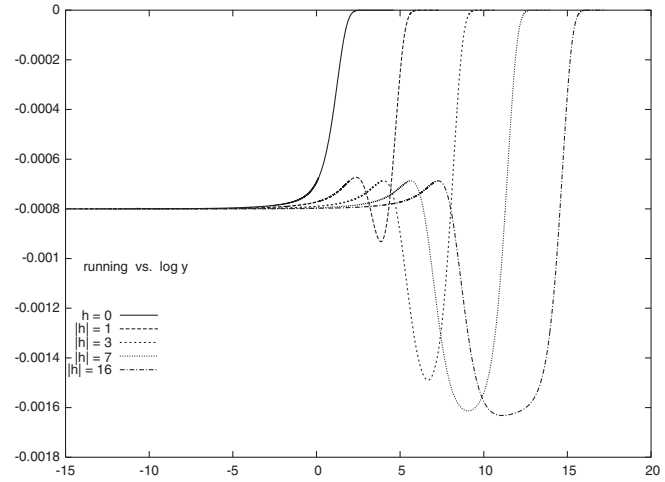

FIG. 2. New Inflation. The running $dn_s/d\ln k$ as a function of log$y$ for the asymmetry of the potential $|h| = 0$, 1, 3, 7 and 16, y being the dimensionless quartic coupling. The $y \to 0$ limiting value $-\frac{2}{N^2} = -0.0008$ is h-independent and corresponds to the monomial potential $\frac{1}{2}m^2\phi^2$.

fixed asymmetry h. In Fig. 6 we plot $n_{s\,\mathrm{maximum}}(h)$ as a function of h. $n_{s\,\mathrm{maximum}}(h)$ monotonically increases with $|h|$ and rapidly reaches its limiting value $n_{s\,\mathrm{maximum}} = 0.961528\ldots$. The corresponding value for r is $r = 0.114769\ldots$. Values $n_s > n_{s\,\mathrm{maximum}} = 0.961528\ldots$ cannot be described by new inflation with the trinomial potential Eqs. (3.1) and (3.2).

We see from Fig. 4 and 5 that both r and the running $dn_s/d\ln k$ are *two*-valued functions of n_s in the interval $0.96 < n_s < 0.961528\ldots$. That is, for each n_s in this range there are *two* possible values for r and for the running $dn_s/d\ln k$. Therefore, we can cover the whole range of values $0.96 < n_s < 0.961\,528\ldots$ choosing the lower

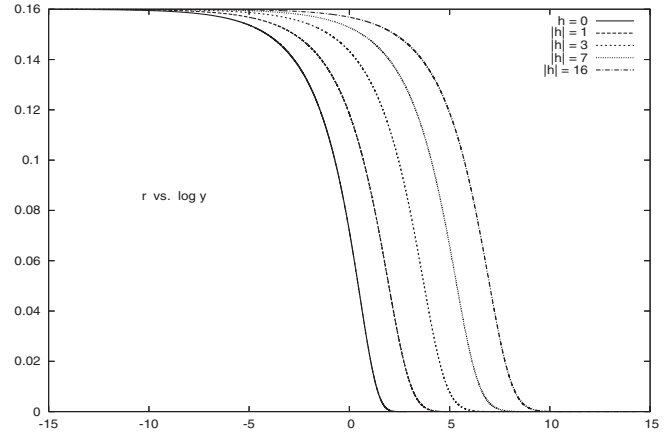

FIG. 3. New Inflation. r as a function of log$y$ for the asymmetry of the potential $|h| = 0$, 1, 3, 7 and 16 y being the dimensionless quartic coupling. The absolute maximum value $r = \frac{8}{N} = 0.16$ is reached for $y = 0$ and all h and corresponds to the monomial potential Eq. (5.2).

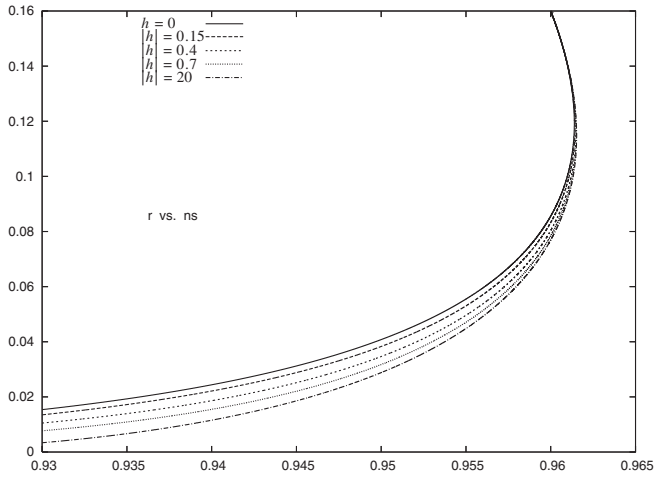

FIG. 4. New Inflation. r as a function of n_s for the asymmetry of the potential $|h| = 0$, 0.15, 0.4, 0.7 and 20. For a given n_s, r monotonically and slowly decreases with increasing $|h|$. $r = r(n_s)$ is not too sensitive to h. The maximum value of n_s is $n_s^{\mathrm{maximum}} = 0.961\,528\ldots$ and the corresponding r is $r_{\max} = 0.114\,769\ldots$. The maximum value of r is $r_{\mathrm{abs\ max}} = 0.16$ and corresponds to the quadratic potential setting $y = 0$ in Eq. (3.2). For $n_s = 0.95$ we find $0.03 < r < 0.04$.

branch for r. We find for this branch

$$r < r_{\max} \equiv 0.114\,769\ldots.$$

This maximum value $r_{\max}$ is well below the absolute

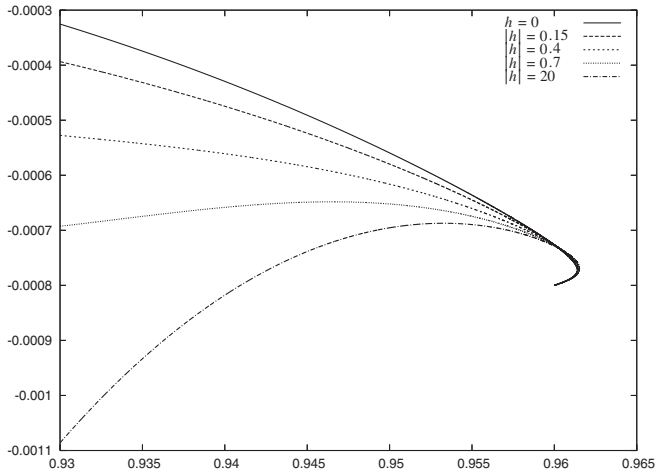

FIG. 5. New Inflation. The running $dn_s/d\ln k$ as a function of n_s for the asymmetry of the potential $|h| = 0$, 0.15, 0.4, 0.7 and 20. The running turns out to be always *negative* in new inflation. For $n_s < 0.96$, the running $dn_s/d\ln k$ decreases with increasing $|h|$. The opposite happens for $n_s > 0.96$. In the last case the dependence on h is weak. We find $dn_s/d\ln k = -0.000\,77\ldots$ at the branch point $n_s = 0.961\ldots$ for all values of $|h|$. The point $n_s = 1 - \frac{2}{N} = 0.96$, $\frac{dn_s}{d\ln k} = -\frac{2}{N^2} = -0.0008$ is reached for all values of h and corresponds to the monomial potential Eq. (5.2). For $n_s = 0.95$, we find $-0.00070 < dn_s/d\ln k < -0.00055$.

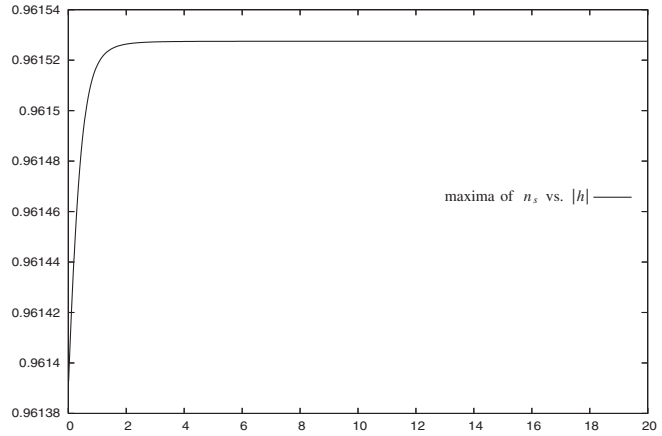

FIG. 6. New Inflation. Maxima of n_s plotted vs the asymmetry of the potential $|h|$. The limiting value for large $|h|$ is $n_s^{\text{maximum}} = 0.961528\ldots$.

maximum in new inflation $r_{\text{abs max}} = 0.16$ [Eq. (4.1)] which belongs to the second branch.

The plots of the ratio r and the running $dn_s/d\ln k$ as a function of n_s show that these quantities are not very sensitive to the asymmetry h for a given value of n_s.

The three years WMAP [5] data as well as ref. [9] yield for n_s the value (see also refs. [10,11])

$$n_s = 0.95 \pm 0.02. \tag{4.2}$$

This value is for the LCDM model and it is obtained with the priors $r = 0$ and $dn_s/d\ln k = 0$.

For $n_s = 0.95$ and any value of the asymmetry h [see Fig. 4], new inflation with the trinomial potential Eqs. (3.1) and (3.2) yields

$$\text{new inflation}: 0.03 < r < 0.04 \quad \text{and}$$
$$-0.000\,70 < dn_s/d\ln k < -0.000\,55.$$

New inflation with the trinomial potential always yield n_s below the maximum value $n_{s\,\text{maximum}} = 0.961\,528\ldots$. For $n_s = 0.961\,528\ldots$ we have in this model $r = 0.114\,769\ldots$. These values of the ratio r fullfil the three years WMAP bound including SDSS galaxy survey [5]

$$r < 0.28(95\%\,\text{CL}). \tag{4.3}$$

Moreover, one can see from fig. 14 in ref. [5] that $r < 0.1(68\%\,\text{CL})$ from WMAP + SDSS.

Chaotic inflation with the trinomial potential Eq. (3.1) and (3.2) yields larger values of r than new inflation for a given value of n_s [8]. More precisely, we find $r = 0.27$ for $n_s = 0.95$ for the binomial potential in chaotic inflation [8] (the trinomial potential introduces very small changes).

Therefore, although the value for n_s [Eq. (4.2)] is compatible both with chaotic and new inflation, the WMAP bounds on r *clearly disfavor* chaotic inflation. New inflation easily fulfils the three years WMAP bounds on r.

The present data do not permit to find the precise values neither of the ratio r nor of the running index $dn_s/d\ln k$; only upper bounds are obtained [4,5]. We therefore think that the value of n_s [Eq. (4.2)] obtained through a fit of the data assuming $r = 0$ is more precise than the values of n_s obtained through fits allowing both r and $dn_s/d\ln k$ to vary. Notice that $n_s = 0.95$ was independently found from the 2dF data under similar assumptions [9].

Ref. [5] reports fits yielding negative values for $dn_s/d\ln k$ of the order ~ -0.05. Notice that the order of magnitude of the running $dn_s/d\ln k$ is just fixed by the fact that it is a second order quantity in slow-roll: $\sim \frac{1}{N^2} \sim 0.0004$. Still, the negative sign of the running reported by Ref. [5] agrees with the sign prediction of new inflation with the trinomial potential [see Fig. 2 and 5].

In summary, new inflation with the trinomial potential Eq. (3.1) and (3.2) predicts $0.03 < r < 0.04$ and $-0.000\,70 < dn_s/d\ln k < -0.000\,55$ for $n_s = 0.95$. For $0.93 < n_s < 0.962$ it predicts $0.01 < r < 0.115$ and $-0.001 < dn_s/d\ln k < -0.0003$ [see Figs. 4 and 5].

V. LIMITING CASES OF THE TRINOMIAL POTENTIAL IN NEW INFLATION

Let us now consider the limiting cases: the shallow limit ($y \to 0$), the steep limit $y \to \infty$ and the extremely asymmetric limit $|h| \to \infty$ of the trinomial potential for new inflation Eqs. (3.1) and (3.2).

A. The shallow limit $y \to 0$ of the Trinomial Potential

In the shallow limit $y \to 0$, z tends to $z = z_+ = (\Delta + |h|)^2$, which is the minimum of y in Eq. (3.4). We find from Eqs. (3.4), (3.5), (3.6), (3.7), and (3.8),

$$n_s \overset{y\to 0}{=} 1 - \frac{2}{N} \simeq 0.96, \qquad \frac{dn_s}{d\ln k} \overset{y\to 0}{=} -\frac{2}{N^2} \simeq -0.0008,$$
$$r \overset{y\to 0}{=} \frac{8}{N} \simeq 0.16, \qquad |\Delta_{k\,\text{ad}}^{(S)}|^2 \overset{y\to 0}{=} \frac{N^2}{3\pi^2}\left(\frac{M}{M_{\text{Pl}}}\right)^4 \Delta(\Delta + |h|), \tag{5.1}$$

which coincide with n_s, $\frac{dn_s}{d\ln k}$ and r for the monomial quadratic potential. That is, the $y \to 0$ limit is h-independent except for $|\Delta_{k\,\text{ad}}^{(S)}|$. For fixed h and $y \to 0$ the inflaton potential Eq. (3.2) becomes purely quadratic:

$$w(\chi) \overset{y\to 0}{=} \Delta(\Delta + |h|)(\chi - \chi_+)^2 + \mathcal{O}(\sqrt{y}), \tag{5.2}$$

where $\chi_+ \equiv (\frac{8}{y})^{1/2}(\Delta + |h|)$. Notice that the amplitude of scalar adiabatic fluctuations Eq. (5.1) turns out to be proportional to the square mass of the inflaton in this regime which we read from Eq. (5.2): $2\Delta(\Delta + |h|)$. The shift of the inflaton field by χ_+ has no observable consequences.

The numerical values in Eq. (5.1) are in agreement with Figs. 1–3 in the $y \to 0$ limit. For $h = 0$ we recover the results of the monomial potential.

B. The steep limit $y \to \infty$ of the trinomial potential

In the steep limit $y \to \infty$, z tends to zero for new inflation. We find from Eq. (3.4)

$$y \overset{z\to 0}{=} -F(h)\log z - q(h) - 1 + \mathcal{O}(\sqrt{z}), \qquad (5.3)$$

where

$$q(h) \equiv 2F(h)\log[\Delta - |h|] - \frac{2}{3}(h^2 + |h|\Delta)\left\{8\Delta^2 \log\left[\frac{1}{2}\left(1 - \frac{|h|}{\Delta}\right)\right] - 1\right\},$$

$q(h)$ is a monotonically increasing function of the asymmetry $|h|$: $0 \le q(h) < \infty$ for $0 < |h| < \infty$.

Then, Eqs. (3.6) and (3.7) yield,

$$n_s \overset{y\gg 1}{=} 1 - \frac{y}{NF(h)}, \qquad r \overset{y\gg 1}{=} \frac{16y}{NF^2(h)} e^{-(y+1+q(h)/F(h))},$$
$$\frac{dn_s}{d\ln k} \overset{y\gg 1}{=} -\frac{2y^2|h|}{N^2F^2(h)} e^{-(y+1+q(h)/2F(h))}, \qquad (5.4)$$
$$|\Delta^{(S)}_{k\,\mathrm{ad}}|^2 \overset{y\gg 1}{=} \frac{N^2}{12\pi^2}\left(\frac{M}{M_{\mathrm{Pl}}}\right)^4 \frac{F^3(h)}{y^2} e^{(y+1+q(h)/F(h))}.$$

In the $h \to 0$ limit we recover from Eqs. (5.3) and (5.4) the results for new inflation with a purely quartic potential: we have $F(0) = 1$ and $q(0) = 0$ and Eq. (5.4) becomes,

$$n_s \overset{y\gg 1, h\to 0}{=} 1 - \frac{y}{N}, \qquad r \overset{y\gg 1, h\to 0}{=} \frac{16y}{N} e^{-y-1},$$
$$\frac{dn_s}{d\ln k} \overset{y\gg 1, h\to 0}{=} -\frac{2y^2|h|}{N^2} e^{-y-1}, \qquad (5.5)$$
$$|\Delta^{(S)}_{k\,\mathrm{ad}}|^2 \overset{y\gg 1, h\to 0}{=} \frac{N^2}{12\pi^2}\left(\frac{M}{M_{\mathrm{Pl}}}\right)^4 \frac{e^{y+1}}{y^2}.$$

The behavior in Eqs. (5.4) is in agreement with Figs. 1–3 in the $y \to +\infty$ limit.

C. The extremely asymmetric limit $|h| \to \infty$ of the trinomial potential

Equations (3.4), (3.5), (3.6), (3.7), and (3.8) have a finite limit for $|h| \to \infty$ with y and z scaling as h^2. Define,

$$Z \equiv \frac{z}{h^2}, \qquad Y \equiv \frac{y}{h^2}.$$

Then, we find for $|h| \to \infty$ from Eqs. (3.4), (3.5), (3.6), (3.7), and (3.8) keeping Z and Y fixed,

$$Y = Z - \frac{4}{3}\sqrt{Z} - 4 - \frac{4}{3}\log\frac{Z}{4} + \frac{16}{3\sqrt{Z}},$$
$$n_s = 1 - 6\frac{Y}{N}\frac{Z^2(\sqrt{Z}-2)^2}{[\frac{16}{3} - \frac{8}{3}Z^{3/2} + Z^2]^2} + \frac{Y}{N}\frac{3Z - 4\sqrt{Z}}{\frac{16}{3} - \frac{8}{3}Z^{3/2} + Z^2}, \qquad (5.6)$$

$$\frac{dn_s}{d\ln k} = -\frac{2}{N^2}Y^2Z\frac{(\sqrt{Z}-2)(\frac{3}{2}\sqrt{Z}-1)}{[\frac{16}{3} - \frac{8}{3}Z^{3/2} + Z^2]^2} - \frac{24}{N^2}Y^2Z^4\frac{(\sqrt{Z}-2)^4}{[\frac{16}{3} - \frac{8}{3}Z^{3/2} + Z^2]^4} + \frac{8}{N^2}Y^2Z^{5/2}\frac{(3\sqrt{Z}-4)(\sqrt{Z}-2)^2}{[\frac{16}{3} - \frac{8}{3}Z^{3/2} + Z^2]^3}, \qquad (5.7)$$

$$r = 16\frac{Y}{N}\frac{Z^2(\sqrt{Z}-2)^2}{[\frac{16}{3} - \frac{8}{3}Z^{3/2} + Z^2]^2}, \qquad (5.8)$$
$$|\Delta^{(S)}_{k\,\mathrm{ad}}|^2 = \frac{N^2h^2}{12\pi^2}\left(\frac{M}{M_{\mathrm{Pl}}}\right)^4 \frac{[\frac{16}{3} - \frac{8}{3}Z^{3/2} + Z^2]^2}{Y^2Z^2(\sqrt{Z}-2)^2}.$$

We have $0 \le Z \le 4$ for $+\infty \ge Y \ge 0$. In the $|h| \to \infty$ limit the inflaton potential takes the form

$$W(\chi) \equiv \lim_{|h|\to\infty}\frac{w(\chi)}{h^2} = \frac{32}{3Y} - \frac{1}{3}\sqrt{\frac{Y}{2}}\chi^3 + \frac{Y}{32}\chi^4. \qquad (5.9)$$

This is a broken symmetric potential without quadratic term. Notice that the cubic coupling has dimension of a mass in Eq. (3.1) and hence this is *not* a massless potential contrary to the quartic monomial χ^4. In addition, Eq. (5.8) shows that for large $|h|$ one must keep the product $|h|M^2$ fixed since it is determined by the amplitude of the adiabatic perturbations. We see from Eq. (5.8) that $\tilde{M} \equiv \sqrt{|h|}M$ becomes the energy scale of inflation in the $|h| \to \infty$ limit. $\tilde{M} \sim 10^{16}$ GeV according to the observed value of $|\Delta^{(S)}_{k\,\mathrm{ad}}|/N$ displayed in Eq. (2.11), while $M = \tilde{M}/\sqrt{|h|}$ vanishes as $|h| \to \infty$.

We have from Eq. (5.9) near the minimum $\chi = \chi_0 = \sqrt{32/Y}$ of $W(\chi)$,

$$W(\chi) \overset{\chi\to\chi_0}{=} 2(\chi - \chi_0)^2.$$

Therefore, the inflaton mass $\sqrt{V''(\phi_0)}$ around the minimum $\phi = \phi_0 = \sqrt{N}M_{\mathrm{Pl}}\chi_0$ takes the finite value,

$$\sqrt{V''(\phi_0)} \overset{|h|\to\infty}{=} 2\frac{\tilde{M}^2}{M_{\mathrm{Pl}}},$$

in the $|h| \to \infty$ limit.

The curves in Figs. 1–6 for high values of $|h|$ are well described by Eq. (5.6).

VI. HYBRID INFLATION

In the inflationary models of hybrid type, the inflaton is coupled to another scalar field σ_0 with mass term $-\mu_0^2 < 0$ through a potential of the type [12]

$$V_{\rm hyb}(\phi,\sigma_0)=\frac{m^2}{2}\,\phi^2+\frac{g_0^2}{2}\,\phi^2\sigma_0^2+\frac{\mu_0^4}{16\Lambda_0}\left(\sigma_0^2-\frac{4\Lambda_0}{\mu_0^2}\right)^2$$
$$=\frac{m^2}{2}\,\phi^2+\Lambda_0+\frac{1}{2}(g_0^2\phi^2-\mu_0^2)\sigma_0^2+\frac{\mu_0^4}{16\Lambda_0}\,\sigma_0^4, \qquad (6.1)$$

where $m^2>0$, $\Lambda_0>0$ plays the role of a cosmological constant and g_0^2 couples σ_0 with ϕ.

The initial conditions are chosen such that σ_0 and $\dot\sigma_0$ are very small (but not identically zero) and therefore one can consider initially,

$$V_{\rm hyb}(\phi,0)=\frac{m^2}{2}\,\phi^2+\Lambda_0. \qquad (6.2)$$

One has then inflation driven by the cosmological constant Λ_0 plus the initial value of the inflaton $\phi(0)$. The inflaton field $\phi(t)$ decreases with time while the scale factor $a(t)$ grows exponentially with time. We see from Eq. (6.1) that

$$m_\sigma^2=g_0^2\phi^2-\mu_0^2, \qquad (6.3)$$

plays the role of a effective classical mass square for the field σ_0. The initial value of m_σ^2 depends on the initial conditions but is typically positive. In any case, since the inflaton field ϕ decreases with time, m_σ^2 will be necessarily negative at some moment during inflation. At such moment, spinodal (tachyonic) instabilities appear and the field σ_0 starts to grow exponentially. Inflation stops when both fields ϕ and σ_0 reach their vacuum values. A matter dominated regime follows.

Normally, the field σ_0 is negligible when the relevant cosmological scales cross out the horizon. Hence, σ_0 does not affect the spectrum of density and tensor fluctuations except through the number of e-folds. Hence, hybrid inflation is a single-field inflationary model as long as ϕ solely contributes to the spectrum of density and tensor fluctuations. However, we find specific regions of parameters (g_0,μ_0,Λ_0) and initial conditions where both fields ϕ and σ_0 contribute to the cosmologically relevant fluctuations making hybrid inflation a two-field inflationary model. We do not consider such regions of parameters here which are outside the scope of this paper.

In terms of the dimensionless fields and couplings, the potential $V_{\rm hyb}(\phi,\sigma_0)$ Eq. (6.1) reads

$$w(\chi,\sigma)=\frac{1}{2}\chi^2+\frac{\mu^4}{8\Lambda}\left(\sigma^2-\frac{2\Lambda}{\mu^2}\right)^2+\frac{1}{2}g^2\sigma^2\chi^2$$
$$=\frac{1}{2}\chi^2+\frac{1}{2}(g^2\chi^2-\mu^2)\sigma^2+\frac{1}{2}\Lambda+\frac{\mu^4}{8\Lambda}\,\sigma^4, \qquad (6.4)$$

where

$$\sigma(\tau)\equiv\frac{\sigma_0(t)}{\sqrt{N}M_{\rm Pl}},\qquad g^2\equiv g_0^2\frac{NM_{\rm Pl}^2}{m^2},$$
$$\mu^2\equiv\frac{\mu_0^2}{m^2}\quad\text{and}\quad\Lambda\equiv\frac{2\Lambda_0}{M^4N}.$$

The evolution equations for this potential in dimensionless variables take the form

$$\mathcal{H}^2(\tau)=\frac{1}{6}\left[\frac{1}{N}\dot\chi^2+\chi^2+\frac{\mu^4}{4\Lambda}\left(\sigma^2-\frac{2\Lambda}{\mu^2}\right)^2+g^2\sigma^2\chi^2\right],$$
$$\left[\frac{1}{N}\frac{d^2}{d\tau^2}+3\mathcal{H}\frac{d}{d\tau}+1+g^2\sigma^2\right]\chi=0,$$
$$\left[\frac{1}{N}\frac{d^2}{d\tau^2}+3\mathcal{H}\frac{d}{d\tau}-\mu^2+g^2\chi^2+\frac{\mu^4}{2\Lambda}\sigma^2\right]\sigma(\tau)=0. \qquad (6.5)$$

Since the field σ is chosen initially very small, it can be neglected and we can approximate the evolution equations (6.5) as

$$3\mathcal{H}\dot\chi+\chi=0,\qquad \mathcal{H}^2(\tau)=\frac{1}{6}[\chi^2+\Lambda]. \qquad (6.6)$$

The number of e-folds from the time τ until the end of inflation is then given by Eq. (2.8),

$$N(\tau)=N\int_\tau^{\tau_{\rm end}}\mathcal{H}(\tau)d\tau=-\int_{\chi(\tau)}^{\chi_{\rm end}}\frac{w(\chi)}{w'(\chi)}d\chi$$
$$=\frac{N}{4}[\chi^2(\tau)-\chi_{\rm end}^2]+\frac{N}{2}\Lambda\log\frac{\chi(\tau)}{\chi_{\rm end}}, \qquad (6.7)$$

$\chi_{\rm end}$ is the inflaton field at the end of inflation.

We see that the inflaton field and its dynamics only appear in $N(\tau)$ Eq. (6.7) through the value of $\chi_{\rm end}$ where inflation stops. The value of $\chi_{\rm end}$ follows by solving Eqs. (6.5) and depends on the initial conditions as well as on the parameters g, μ and Λ.

The spectral indices are given by Eqs. (2.10) and the amplitude of adiabatic perturbations by Eq. (2.9). By using the potential equation (6.2) in dimensionless variables we find,

$$w(\chi,0)=\frac{1}{2}(\chi^2+\Lambda),$$
$$|\Delta_{k\,\rm ad}^{(S)}|^2=\frac{N^2}{96\pi^2}\left(\frac{M}{M_{\rm Pl}}\right)^4\frac{(\chi^2+\Lambda)^3}{\chi^2}, \qquad (6.8)$$
$$r=\frac{32}{N}\,\frac{\chi^2}{(\chi^2+\Lambda)^2},$$

$$n_s=1+\frac{4}{N}\,\frac{\Lambda-2\chi^2}{(\chi^2+\Lambda)^2},\qquad \frac{dn_s}{d\ln k}=\frac{32}{N^2}\,\frac{\chi^2(2\Lambda-\chi^2)}{(\chi^2+\Lambda)^4}, \qquad (6.9)$$

where χ is the inflaton at the moment of the first horizon crossing.

VII. INFLATON DYNAMICS IN HYBRID INFLATION

In Figs. 7–11 we display the numerical solution of the equations of motion (6.5) as functions of time for $\Lambda = 4N = 200$, $\mu^2 = 1.7\Lambda$, $\phi(0) = 2.3\sqrt{\Lambda}$. We see first a stage of slow-roll quasi-de Sitter inflation until $\tau \simeq 39$ in this example. Namely, $|\dot{\phi}| \ll |\phi|$ and h are practically constant during this lapse. In this slow-roll stage the equations of motion (6.6) can be integrated in close form with the solution

$$\sqrt{\frac{2}{3\Lambda}}(\tau - \tau_0) = \arg\tanh\frac{1}{\sqrt{1+\frac{\chi^2}{\Lambda}}} - \sqrt{1+\frac{\chi^2}{\Lambda}}, \qquad (7.1)$$

which defines $\chi = \chi(\tau)$ and where τ_0 is an integration constant. Notice that $\chi(\tau)$ is a monotonically decreasing function of time since $\dot{\chi} = -\chi/[3h] < 0$ [Eq. (6.6)].

When $\chi \ll \Lambda$, Eq. (7.1) approximates by

$$\chi(\tau) \simeq \chi_0 e^{-\sqrt{2/3\Lambda}\tau}, \qquad \chi \ll \Lambda,$$

while in the opposite limit $\chi \gg \Lambda$ from Eq. (7.1) we have,

$$\chi(\tau) \simeq \chi_1 - \sqrt{\frac{2}{3}}\tau, \qquad \chi \gg \Lambda.$$

Here, χ_0 and χ_1 are integration constants.

We have verified that Eq. (7.1) as well as Eq. (6.7) provide an excellent approximation to the numerical solution of Eqs. (6.5).

The number of e-folds during inflation is about 280 in the example depicted in Figs. 7–11, larger than the required minimum of about 60 e-folds. This stage is followed by a matter dominated era. We choose a very small initial amplitude for the sigma field and its time derivative. The sigma field stays very small until its effective mass square [Eq. (6.3)] becomes negative and spinodal instabilities show up. At this moment, ($\tau \simeq 4$ in this example) the sigma field as well as its time derivative start to increase exponentially fast until the growth of the nonlinear term $+\frac{\mu^4}{2\Lambda}\sigma^2$ in the last equation in Eq. (6.5) shuts off the instabilities.

Inflation stops at the moment when both χ and σ are comparable with $\dot{\chi}$ and $\dot{\sigma}$ ($\tau \simeq 39$ in this example). At this time, both χ and σ are very close to their vacuum values $\chi_{\rm vac} = 0$ and $\sigma_{\rm vac} = \frac{\sqrt{2\Lambda}}{\mu}$. That is, when the kinetic terms

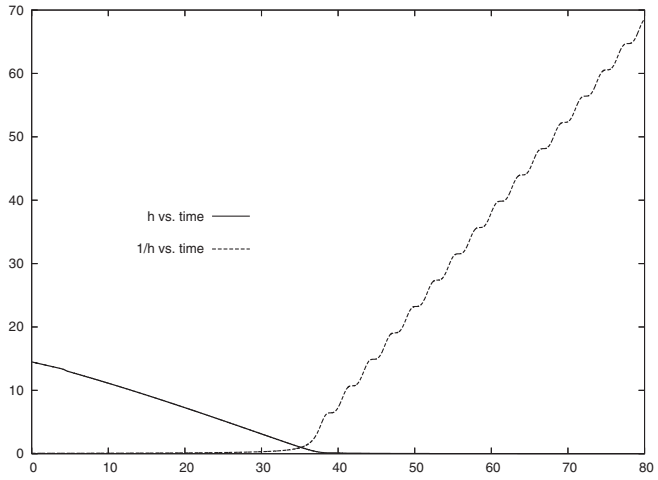

FIG. 8. Hybrid inflation. The Hubble parameter h and its inverse $1/h$ as a function of time. Same parameters as in Fig. 7. h slowly decreases with time in the slow-roll quasi-de Sitter stage (until $\tau \simeq 39$ in this example) followed by $h \simeq 2/[3\tau]$ in the matter dominated era.

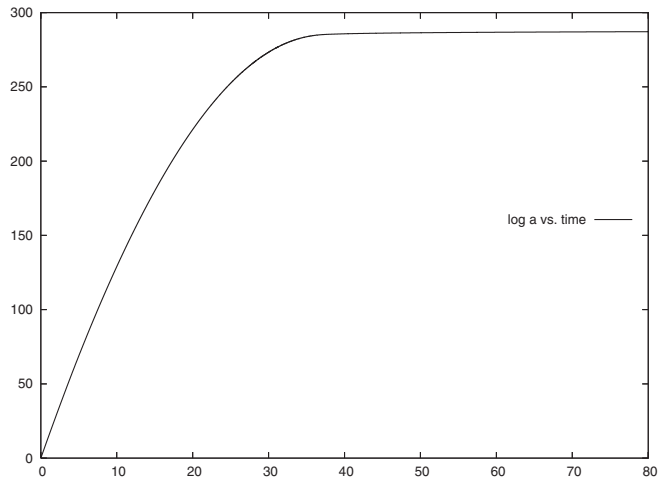

FIG. 7. Hybrid inflation. The logarithm of the scale factor (the number of efolds) as a function of time. The chosen parameters in Eq. (6.5) are $\Lambda = 4N = 200$, $\mu^2 = 1.7\Lambda$, $\phi(0) = 2.3\sqrt{\Lambda}$. A stage of slow-roll quasi-de Sitter inflation takes place (until $\tau \simeq 39$ in this example) followed by a matter dominated era.

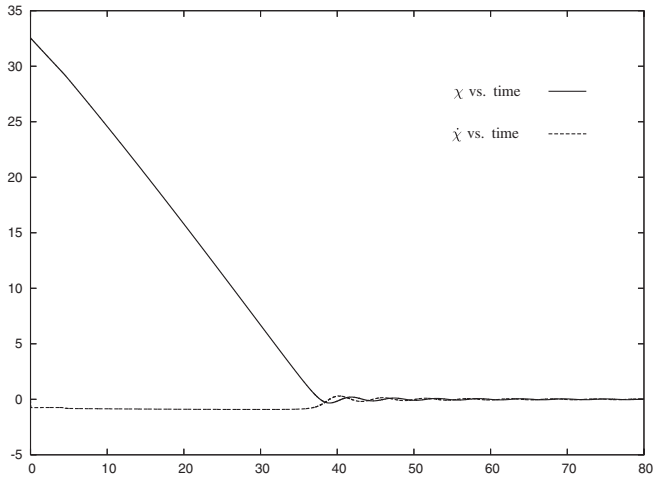

FIG. 9. Hybrid inflation. The inflaton field χ and its time derivative as a function of time. Same parameters as in Fig. 7. $|\dot{\chi}| \ll |\chi|$ during the slow-roll inflationary stage. Inflation stops when $\chi \sim \dot{\chi} \sim 0$ (at $\tau \simeq 39$ in this example).

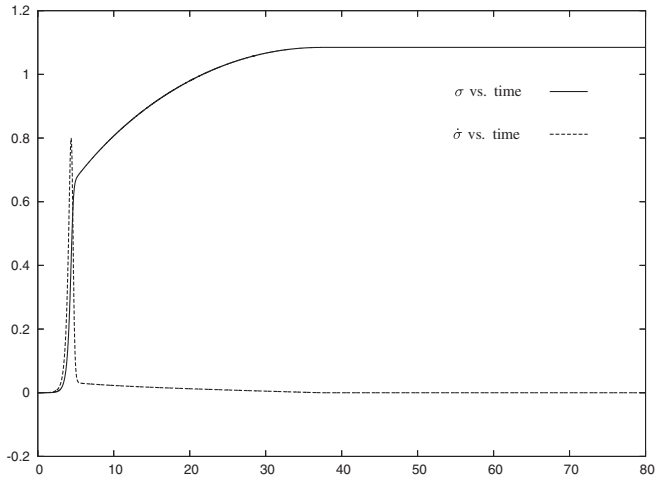

FIG. 10. Hybrid inflation. The field sigma σ and its time derivative as a function of time for hybrid inflation. Same parameters as in Fig. 7. The fields σ and $\dot{\sigma}$ start with small values and grow exponentially fast when $m_\sigma^2 < 0$ [Eq. (7.2)] (at $\tau \simeq 4$ in this example).

become relevant, the energy is no more dominated by the vacuum energy. At the same time, the slow-roll approximation ceases to be valid.

The time when the effective mass of the field σ [see Eq. (6.3)]

$$m_\sigma^2 = m^2(g^2\chi^2 - \mu^2) \tag{7.2}$$

becomes negative and σ starts to grow depends on the values of μ^2 and $g^2\chi^2(0)$. For low values of μ^2: (typically for $\mu^2 < 0.08\Lambda$ when $\chi^2(0) < \Lambda$, and $\mu^2 < 0.2\Lambda$ when $\chi^2(0) < 2.\Lambda$), the field σ starts to grow close to the end of inflation. On the contrary, for higher values of μ^2 (typically for $\mu^2 > 0.08\Lambda$ when $\chi^2(0) < \Lambda$, and $\mu^2 > 0.23\Lambda$ when $\chi^2(0) < 2.\Lambda$), the field σ starts to grow well before the end of inflation. This is explained by the fact that the scale of time variation of σ goes as μ^{-1}; σ evolves slowly for small μ and quickly for large μ.

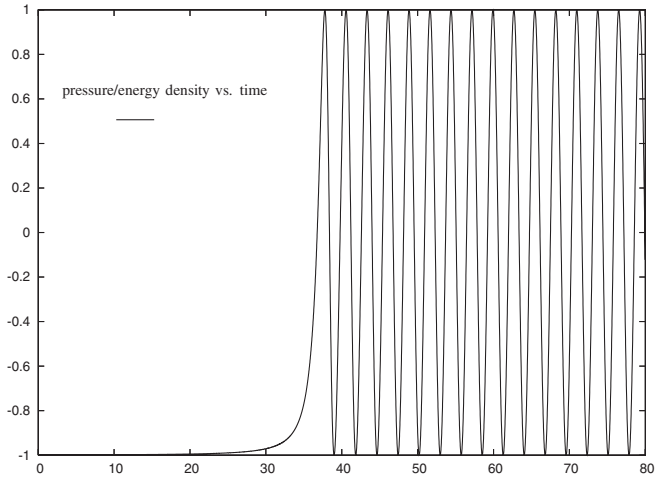

FIG. 11. Hybrid inflation. The equation of state pressure/energy density as a function of time. Same parameters as in Fig. 7. The equation of state clearly shows the two stages: pressure/energy $= -1$ during inflation followed by oscillations with zero average pressure in the matter dominated era.

$\dot{\sigma}$ exhibits a peak around the point where m_σ^2 changes sign and then returns to a very small value while σ slowly approaches its vacuum value. This evolution is depicted in Fig. 10.

In the example depicted in Figs. 7–11 the effective mass square [Eq. (7.2)] of the σ field changes sign at $\tau \sim 4$ well before χ reaches its vacuum value (zero) and inflation ends. This follows from the choice of a large value for μ^2 in Figs. 7–11. For smaller values of μ^2, m_σ^2 [Eq. (7.2)] flips its sign later when the inflaton χ is much smaller.

In order to compute the observables n_s, r and $dn_s/d\ln k$ from Eq. (6.8) we need the value of the inflation field χ at 50 e-folds before the end of inflation. We thus integrated numerically Eqs. (6.5) until the end of inflation and then extracted the value of χ at 50 e-folds before. We define the end of inflation as the point where the ratio pressure over energy reaches 10%. This gives $\tau \equiv \tau_{\rm end} \simeq 34$ for the example in Fig. 11.

At $\Lambda = 0$ hybrid inflation becomes chaotic inflation with the monomial potential $\frac{1}{2}\chi^2$. We want to stress that only *at* $\Lambda = 0$ hybrid inflation becomes chaotic inflation. For any value of $\Lambda > 0$ (even very small) the features of hybrid inflation remain. The time $\tau_{\rm end}$ gets longer and longer for $\Lambda \to 0^+$.

VIII. SPECTRAL INDEX n_s, RATIO r AND RUNNING INDEX $\frac{dn_s}{d\ln k}$ IN HYBRID INFLATION

We see from Eqs. (6.9) that the field χ naturally scales as $\sqrt{\Lambda}$. It is then convenient to introduce the rescaled field and the rescaled mass

$$\hat{\chi} \equiv \frac{\chi}{\sqrt{\Lambda}}, \qquad \hat{\mu}^2 \equiv \frac{\mu^2}{\Lambda}. \tag{8.1}$$

Then, Eqs. (6.9) take the form

$$\begin{aligned} w(\chi, 0) &= \frac{\Lambda}{2}(\hat{\chi}^2 + 1), \\ |\Delta^{(S)}_{k\,\rm ad}|^2 &= \frac{N^2\Lambda^2}{96\pi^2}\left(\frac{M}{M_{\rm Pl}}\right)^4 \frac{(\hat{\chi}^2+1)^3}{\hat{\chi}^2}, \\ r &= \frac{32}{N\Lambda}\,\frac{\hat{\chi}^2}{(\hat{\chi}^2+1)^2}, \end{aligned} \tag{8.2}$$

$$n_s = 1 + \frac{4}{N\Lambda}\,\frac{1-2\hat{\chi}^2}{(\hat{\chi}^2+1)^2}, \qquad \frac{dn_s}{d\ln k} = \frac{32}{N^2\Lambda^2}\,\frac{\hat{\chi}^2(2-\hat{\chi}^2)}{(\hat{\chi}^2+1)^4}. \tag{8.3}$$

Notice that $(n_s - 1)$ may have either sign according to Eq. (8.3). Hybrid inflation is usually associated with red

tilted spectrum ($n_s > 1$). However, both regimes, $n_s > 1$ *and* $n_s < 1$ are realized by hybrid inflation.

Whether $n_s > 1$ or $n_s < 1$ for a given set of parameters Λ, μ^2, g and the initial conditions is a *dynamical* question that can only be answered after evolving the fields until the end of inflation according to Eqs. (6.5). As we see in Eq. (6.9) the question is whether twice χ^2 at horizon exit is larger or smaller than Λ. Recall that horizon exit happens about 50 e-folds before the end of inflation and that χ^2 monotonically decreases during inflation. Even if initially $2\chi^2 > \Lambda$, it can be very well that $2\chi^2 < \Lambda$ at horizon exit. This depends on how many total e-folds $N_T \geq 60$ we have; since horizon exit happens $(N_T - 50) \geq 10$ e-folds after the beginning of inflation, the larger is $(N_T - 50)$ the smaller can be χ^2 at horizon exit.

We vary the parameters Λ, μ^2 and the initial conditions always keeping the total number of e-folds N_T during inflation larger or equal to 60. We keep $g^2 = \frac{1}{4}$ since this parameter is less relevant than the others. We explored the parameters region where $r < 0.2$ and $0.95 < n_s < 1.15$.

A. Red tilted and blue tilted regimes in hybrid inflation

Extended numerical investigation showed that there exists a *critical value* of μ^2, $\mu^2_{\rm crit} \simeq 0.13\Lambda$ such that $n_s > 1$ provided $\mu^2 < \mu^2_{\rm crit}$.

For $\mu^2 > \mu^2_{\rm crit}$ we find both regimes, $n_s > 1$ *and* $n_s < 1$. This property is valid for all initial values of the inflaton compatible with the restrictions $N_T \geq 60$ and one-inflaton fluctuations. Otherwise, if the field σ is relevant at horizon exit we should also include its contribution to the density fluctuations. Such calculation is beyond the scope of the present work where we concentrate on single inflaton fluctuations.

The larger is μ^2, the earlier inflation ends, the earlier horizon exit happens and the large is χ at horizon exit. That is, increasing μ^2 decreases n_s. This explains why we necessarily find $n_s < 1$ for $\mu^2 > \mu^2_{\rm crit}$.

For $\mu^2 > \mu^2_{\rm crit}$ we find that $n_s > 1$ for $\chi(0) > \chi(0)_{\rm crit}$. That is, increasing $\chi(0)$, increases n_s. This is so because the larger is $\chi(0)$, the larger is N_T since $N_T \sim \chi(0)^2$ [see Eqs. (6.6) and (6.7)]. Then, the larger is $(N_T - 50)$ the smaller is χ at horizon exit and the larger is n_s.

In all cases, (both $\mu^2 > \mu^2_{\rm crit}$ and $\mu^2 < \mu^2_{\rm crit}$) for $\Lambda \to \infty$ we always find $n_s \to 1$, $r \to 0$ and $\frac{dn_s}{d\ln k} \to 0$.

Figures 12–23 show the observables n_s, r and the running index $dn_s/d\ln k$ as functions of Λ and n_s for $\mu^2 = 0.05\Lambda$, $\mu^2 = 0.13\Lambda$ and $\mu^2 = 1.7\Lambda$. A complete picture for hybrid inflation emerges covering *two* different, blue tilted and red tilted, regimes. We find that for all the observables, the shape of the curves depends crucially on the mass parameter $\hat{\mu}^2$ of the σ field and the (rescaled) initial amplitude $\hat{\chi}(0)$ of the inflaton field.

We find three regimes according to the value of $\hat{\mu}^2$:

(i) $\hat{\mu}^2 < 0.075$. Here we always have $n_s > 1$ and r has one maximum as a function of n_s (or Λ). n_s monotonically decreases with Λ. Figures 12 and 13 show r vs n_s for $\mu^2 = 0.05\Lambda$ and various values of $\hat{\chi}(0)$. r displays a maximum as a function of n_s. In addition, r grows with $\hat{\chi}(0)$ for $\hat{\chi}(0) < 0.5$ while it decreases with $\hat{\chi}(0)$ for $\hat{\chi}(0) > 0.5$. The running $\frac{dn_s}{d\ln k}$ behavior is qualitatively similar to the behavior of r above described. The running $\frac{dn_s}{d\ln k}$ is here positive and grows when n_s grows.

(ii) $0.075 < \hat{\mu}^2 < \hat{\mu}^2_{\rm crit} \simeq 0.13$. Here we always have $n_s > 1$ and r monotonically grows with Λ. n_s monotonically decreases with Λ for $\hat{\mu}^2 < 0.1$ while it exhibits a maximum as a function of Λ

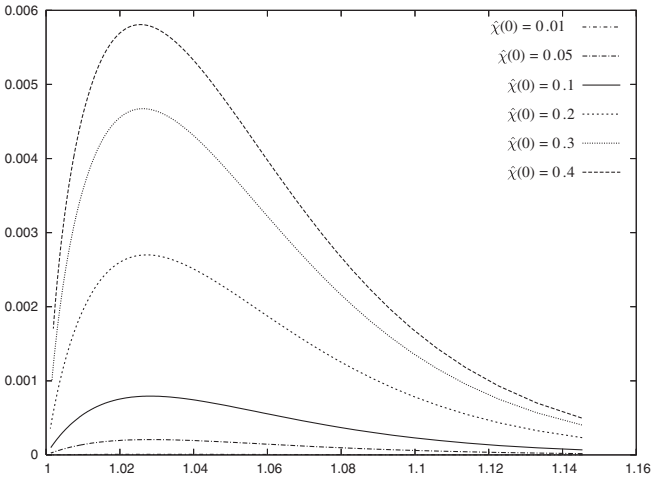

FIG. 12. Hybrid inflation. The ratio r vs n_s for $\mu^2 = 0.05\Lambda < \mu^2_{\rm crit}$ and $0.01\sqrt{\Lambda} \leq \chi(0) \leq 0.4\sqrt{\Lambda}$. Notice that here r has a maximum as a function of n_s. In addition, $n_s > 1$ for all values of Λ and $\hat{\chi}(0)$ since $\mu^2 < \mu^2_{\rm crit} \simeq 0.13\Lambda$. r increases with $\hat{\chi}(0)$ for this range of $\hat{\chi}(0)$.

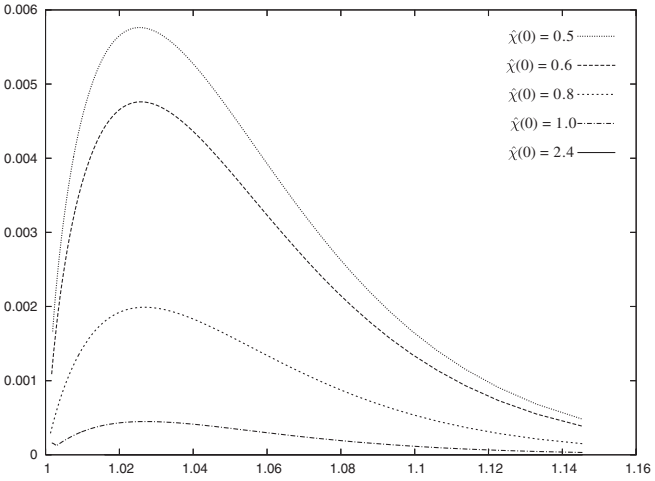

FIG. 13. Hybrid inflation. The ratio r vs n_s for $\mu^2 = 0.05\Lambda < \mu^2_{\rm crit}$, $g^2 = \frac{1}{4}$ and $0.5\sqrt{\Lambda} \leq \chi(0) \leq 2.4\sqrt{\Lambda}$. Notice that here r has a maximum as a function of n_s. In addition, $n_s > 1$ for all values of Λ and $\chi(0)$ since $\mu^2 < \mu^2_{\rm crit} \simeq 0.13\Lambda$. r decreases with $\hat{\chi}(0)$ for this range of $\hat{\chi}(0)$.

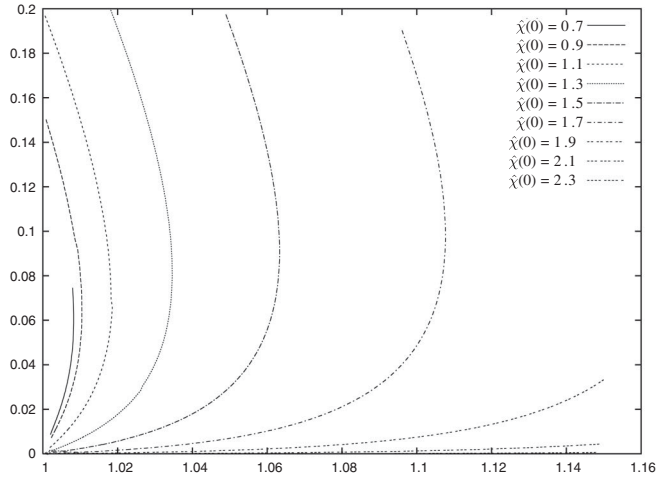

FIG. 14. Hybrid inflation. The ratio r vs n_s for $\mu^2 = 0.13\Lambda \simeq \mu^2_{\rm crit}$, $g^2 = \frac{1}{4}$ and $0.7\sqrt{\Lambda} \leq \chi(0) \leq 2.3\sqrt{\Lambda}$. Notice that here $n_s > 1$ for all values of Λ and $\chi(0)$.

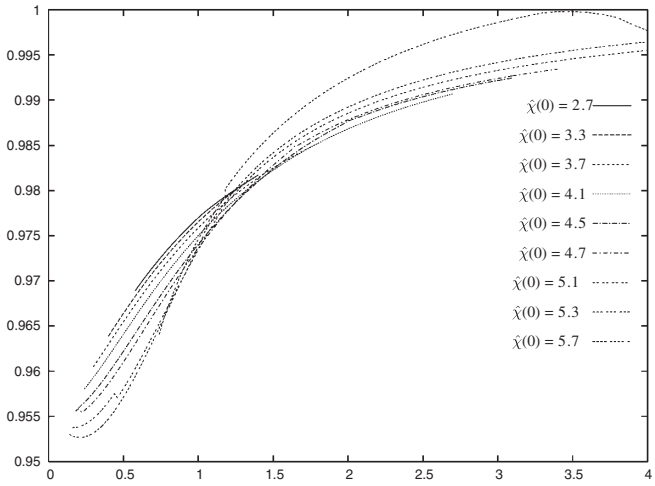

FIG. 16. Hybrid inflation. The index n_s vs Λ for $\mu^2 = 1.7\Lambda > \mu^2_{\rm crit}$, $g^2 = \frac{1}{4}$ and $2.7\sqrt{\Lambda} \leq \chi(0) \leq 5.7\sqrt{\Lambda} \simeq \chi(0)_{\rm crit}$. Notice that here $n_s < 1$ for all values of Λ and this range of $\chi(0)$.

for $\hat{\mu}^2 > 0.1$. Figures 14 and 15 depict r and the running $\frac{dn_s}{d\ln k}$ vs n_s, respectively, for $\hat{\mu}^2 = 0.13 \simeq \hat{\mu}^2_{\rm crit}$. We see that the running $\frac{dn_s}{d\ln k}$ behavior is qualitatively similar to the one of r.

(iii) $\hat{\mu}^2 > 0.13 \simeq \hat{\mu}^2_{\rm crit}$. Here $n_s > 1$ for $\hat{\chi}(0) > \hat{\chi}(0)_{\rm crit}$ and $n_s < 1$ for $\hat{\chi}(0) < \hat{\chi}(0)_{\rm crit}$.
The value of $\hat{\chi}(0)_{\rm crit}$ grows with $\hat{\mu}^2$: for $\hat{\mu}^2 = 0.5$, we find $\hat{\chi}(0)_{\rm crit} = 2.7$ and for $\hat{\mu}^2 = 1.7$, we find $\hat{\chi}(0)_{\rm crit} = 5.8$.
For $\hat{\chi}(0) < \hat{\chi}(0)_{\rm crit}$, n_s monotonically increases with Λ with values $n_s < 1$. For $\hat{\chi}(0) > \hat{\chi}(0)_{\rm crit}$, n_s shows an absolute *maximum*, which is always $n_{s\ \rm max} > 1$. The highest n_s values concentrate and narrow in the small Λ region. It must be noticed that for each curve, [each $\hat{\chi}(0)$], n_s can take values $n_s > 1$ *and* $n_s < 1$: even if $n_{s\ \rm max} > 1$, n_s can be below unit in the two sides of the curve, [see Figs. 16 and 17].
The value $n_s = 1$, is reached asymptotically for large Λ from $n_s < 1$ for both $\hat{\chi}(0) < \hat{\chi}(0)_{\rm crit}$ and $\hat{\chi}(0) > \hat{\chi}(0)_{\rm crit}$. In addition, the value $n_s = 1$ with $0.2 > r > 0.04$ is found for a variety of values of Λ and $\hat{\chi}(0) > \hat{\chi}(0)_{\rm crit}$ as we see from Figs. 17, 19, and 21.

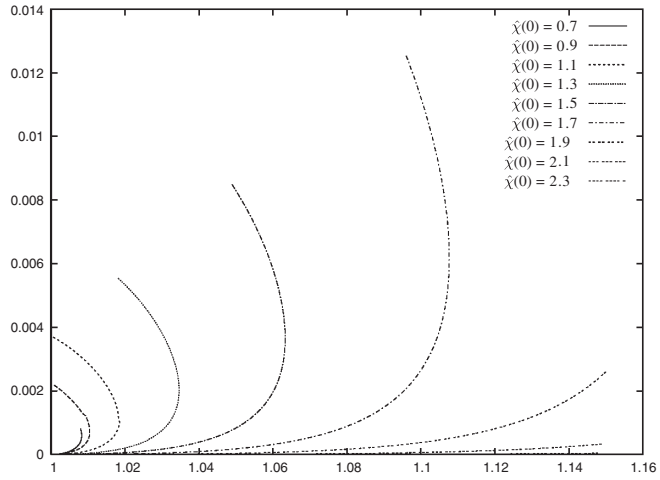

FIG. 15. Hybrid inflation. The running $dn_s/d\ln k$ vs n_s for $\mu^2 = 0.13\Lambda \simeq \mu^2_{\rm crit}$, $g^2 = \frac{1}{4}$ and $0.7\sqrt{\Lambda} \leq \chi(0) \leq 2.3\sqrt{\Lambda}$. Notice that here $dn_s/d\ln k > 0$ for all values of Λ and $\chi(0)$. It exhibits a shape similar to r vs n_s [see Fig. 13].

B. The ratio r in hybrid inflation

The ratio r in Figs. 18 and 19 exhibits an *oscillatory* pattern and two different regimes:

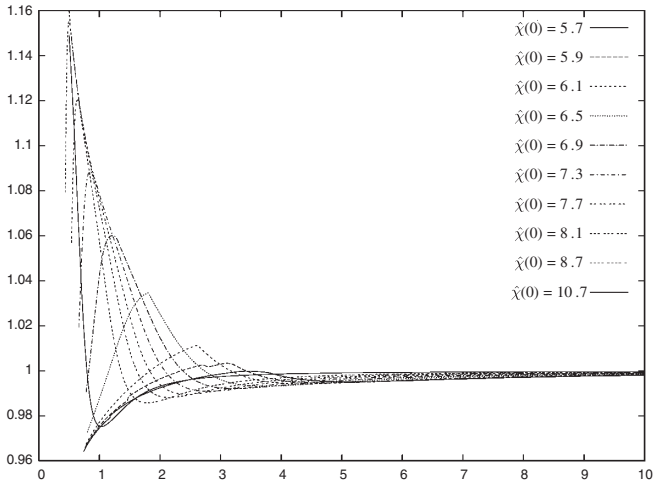

FIG. 17. Hybrid inflation. The index n_s vs Λ for $\mu^2 = 1.7\Lambda > \mu^2_{\rm crit}$, $g^2 = \frac{1}{4}$ and $\chi(0)_{\rm crit} \simeq 5.7\sqrt{\Lambda} \leq \chi(0) \leq 10.7\sqrt{\Lambda}$. Notice that here we have both $n_s > 1$ and $n_s < 1$ depending on the values of Λ and $\hat{\chi}(0)$. All curves reach asymptotically $n_s = 1$ for $\Lambda \to \infty$.

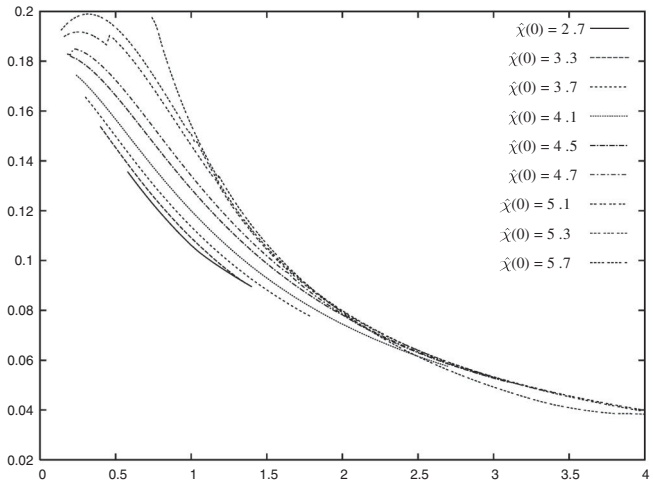

FIG. 18. Hybrid inflation. The ratio r vs Λ for $\mu^2 = 1.7\Lambda > \mu^2_{\rm crit}$, $g^2 = \frac{1}{4}$ and $2.7\sqrt{\Lambda} \leq \chi(0) \leq 5.7\sqrt{\Lambda} \simeq \chi(0)_{\rm crit}$. r decreases monotonically with Λ in this regime $\chi(0) < \chi(0)_{\rm crit}$ and asymptotically vanishes for $\Lambda \to \infty$.

For $\hat{\chi}(0) < \hat{\chi}(0)_{\rm crit}$, (Fig. 18) r decreases monotonically reaching very small values for large Λ. For $\hat{\chi}(0) < \hat{\chi}(0)_{\rm crit}$, r does not feature any oscillation.

For $\hat{\chi}(0) > \hat{\chi}(0)_{\rm crit}$, r decreases with Λ, (Fig. 19) r has an absolute *minimum* $r_{\rm min}$ and then grows until a *maximum*, $r_{\rm max}$. The oscillations show up and concentrate with growing amplitude for small Λ for high $\hat{\chi}(0)$, $r_{\rm min}$ and $r_{\rm max}$ shift towards the smaller Λ with increasing $\hat{\chi}(0)$; $r_{\rm min}$ decreases, and $r_{\rm max}$ increases, for increasing $\hat{\chi}(0)$. The convexity of the curve for small Λ increases for decreasing $\hat{\chi}(0)$.

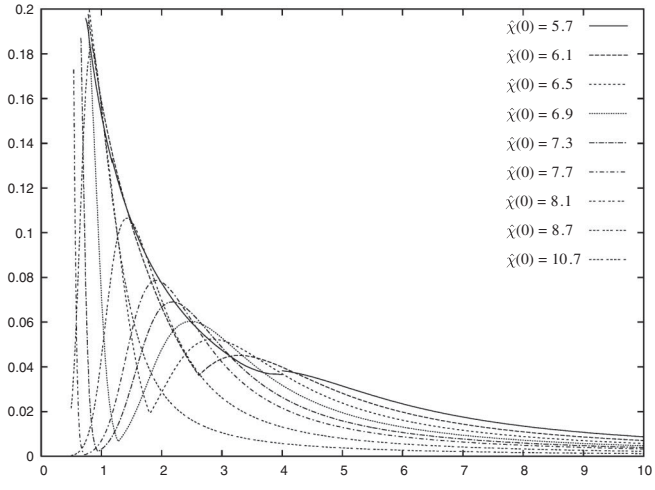

FIG. 19. Hybrid inflation. The ratio r vs Λ for $\mu^2 = 1.7\Lambda > \mu^2_{\rm crit}$, $g^2 = \frac{1}{4}$ and $\chi(0)_{\rm crit} \simeq 5.7\sqrt{\Lambda} \leq \chi(0) \leq 10.7\sqrt{\Lambda}$. r shows an oscillatory pattern in this regime $\chi(0) \geq \chi(0)_{\rm crit}$ and asymptotically vanishes for $\Lambda \to \infty$ with no oscillations. The oscillations show up and concentrate with increasing amplitude for small Λ.

For $\hat{\chi}(0) > \hat{\chi}(0)_{\rm crit}$, each curve [each $\hat{\chi}(0)$] shows for r a *oscillatory* behavior with three clear parts: (1) the asymptotic part of monotonically decreasing r for large Λ at the right of $r_{\rm max}$; (2) the increasing part at the left of $r_{\rm max}$; (3) the sharp decreasing part for small Λ at the left of $r_{\rm min}$. In the minima, $r_{\rm min}$ can be extremely small for small Λ, which is a *new feature* in hybrid inflation.

In the asymptotic regime of large Λ, r does not feature any oscillation. All curves [for all $\hat{\chi}(0)$] coalesce into $r = 0$ for $\Lambda \to \infty$.

There are three distinct regimes: small Λ, intermediate Λ and large Λ. The new oscillatory behavior for high and intermediate $\hat{\chi}(0) > \hat{\chi}(0)_{\rm crit}$ is in the region of small and intermediate Λ. The monotonically decreasing behavior for low $\hat{\chi}(0) < \hat{\chi}(0)_{\rm crit}$ is in the asymptotic region of large Λ.

The highest values of r appear for small Λ whatever be the hybrid regime; for such high values of r both regimes $\hat{\chi}(0) < \hat{\chi}(0)_{\rm crit}$ and $\hat{\chi}(0) > \hat{\chi}(0)_{\rm crit}$ superpose. From such high values, r decreases sharply until its minimum $r_{\rm min}$ in the small Λ region for $\hat{\chi}(0) > \hat{\chi}(0)_{\rm crit}$; or r decreases monotonically reaching asymptotically the large Λ regime for $\hat{\chi}(0) < \hat{\chi}(0)_{\rm crit}$. The low values of r for low Λ are a *totally new* feature in hybrid inflation.

C. The running index $dn_s/d\ln k$ in hybrid inflation

The curves of the running index $dn_s/d\ln k$ Figs. 15, 22, and 23 show *new* features in two different regimes.

For $\hat{\chi}(0) > \hat{\chi}(0)_{\rm crit}$, the running index $dn_s/d\ln k$ shows a similar shape as r and is essentially positive. It oscillates with at least one *maximum* and one or two *minima* and three different components: (1) the asymptotic part of monotonically decreasing running with increasing Λ, at the right of the maximum, going to zero in this regime; (2) the increasing running with Λ, which is a new feature in hybrid inflation, and (3) the sharp decreasing of the running until its minimum value for small Λ. The highest running appears for small Λ as in the known hybrid regime. The lower running values for small Λ, as well as the *oscillations* for small and intermediate Λ, are totally *new.*

For low $\hat{\chi}(0) < \hat{\chi}(0)_{\rm crit}$ the running index does not exhibit any oscillation. Both for $\hat{\chi}(0) < \hat{\chi}(0)_{\rm crit}$ and $\hat{\chi}(0) > \hat{\chi}(0)_{\rm crit}$ $dn_s/d\ln k$ grows with Λ until it reaches its maximum and then decreases monotonically with Λ. $dn_s/d\ln k$ vanishes asymptotically for large Λ without any oscillation. This is a totally *new* feature for hybrid inflation.

Thus, hybrid inflation describes both $dn_s/d\ln k > 0$ and $dn_s/d\ln k < 0$. It must be noticed that $dn_s/d\ln k < 0$ can reach very low values for *small* Λ which is a *totally new* feature in hybrid inflation.

In summary, the *new* features for the running index in hybrid inflation are: both positive and negative running, increasing of the running with Λ, transition from positive to negative running passing through zero running when Λ grows.

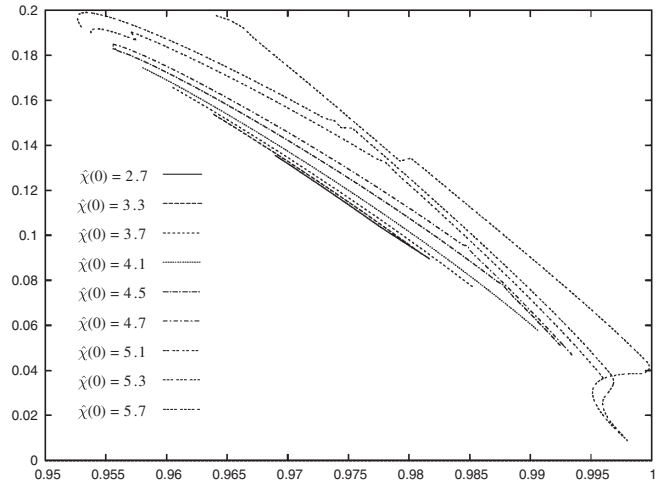

FIG. 20. Hybrid inflation. The ratio r vs n_s for $\mu^2 = 1.7\Lambda > \mu^2_{\rm crit}$, $g^2 = \frac{1}{4}$ and $2.7\sqrt{\Lambda} \leq \chi(0) \leq 5.7\sqrt{\Lambda} \simeq \chi(0)_{\rm crit}$. Notice that here $n_s < 1$ for all values of Λ and this range of $\hat{\chi}(0)$. We see that $0.2 > r > 0.14$ for the interval $0.952 < n_s < 0.97$.

D. r vs n_s. confrontation of hybrid inflation to the three years WMAP data

r vs n_s in Figs. 20 and 21 depicts a oscillatory behavior clearly showing the two regimes: $\hat{\chi}(0) > \hat{\chi}(0)_{\rm crit}$ corresponding mainly to $n_s > 1$, although it also covers a small portion of $n_s < 1$, and $\hat{\chi}(0) < \hat{\chi}(0)_{\rm crit}$ for which n_s is entirely red tilted.

All curves end $[\hat{\chi}(0) < \hat{\chi}(0)_{\rm crit}]$, or start $[\hat{\chi}(0) > \hat{\chi}(0)_{\rm crit}]$, at $n_s = 1$, which is the *fixed* point for all $\hat{\chi}(0)$, with three different behaviors:

(1) the sharp decreasing of r in the range $n_s < 1$, approaching $n_s = 1$ as the end point, this is for $\hat{\chi}(0) < \hat{\chi}(0)_{\rm crit}$, in which r can take high values for small n_s, (n_s near 0.95).

(2) the monotonically decreasing of r with n_s at the right of $r_{\rm max}$, for $\hat{\chi}(0) > \hat{\chi}(0)_{\rm crit}$, in which r vanishes asymptotically for "high" n_s, ($n_s > 1.07$).

(3) The *new* hybrid behavior for high $\hat{\chi}(0) > \hat{\chi}(0)_{\rm crit}$ in between the above two regimes, in which r shows a maximum and a minimum between two sharp decreasing and increasing "arms", lying at $n_s < 1$ and $n_s > 1$ respectively. $r_{\rm min}$ decreases and $r_{\rm max}$ increases as increasing $\hat{\chi}(0)$. All $r_{\rm max}$ lie in the red tilted regime $n_s < 1$. All $r_{\rm min}$ lie in the blue tilted regime $n_s > 1$.

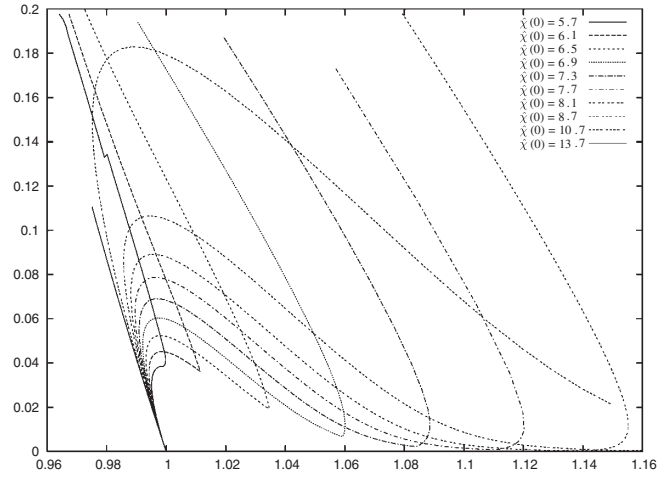

FIG. 21. Hybrid inflation. The ratio r vs n_s for $\mu^2 = 1.7\Lambda > \mu^2_{\rm crit}$, $g^2 = \frac{1}{4}$ and $\chi(0)_{\rm crit} \simeq 5.7\sqrt{\Lambda} \leq \chi(0) \leq 13.7\sqrt{\Lambda}$. Notice that we have here both $n_s > 1$ and $n_s < 1$ depending on the values of Λ and $\hat{\chi}(0)$. All curves end $[\hat{\chi}(0) < \hat{\chi}(0)_{\rm crit}]$ or start $[\hat{\chi}(0) > \hat{\chi}(0)_{\rm crit}]$ at $n_s = 1$ which is the fixed point for all values of $\hat{\chi}(0)$.

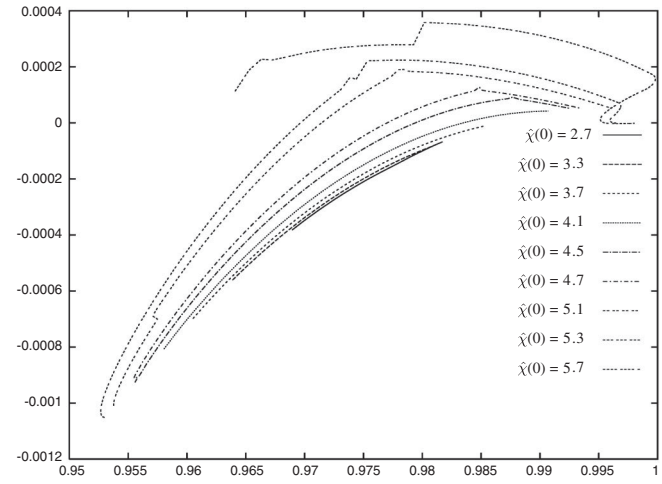

FIG. 22. Hybrid inflation. The running $dn_s/d\ln k$ vs n_s for $\mu^2 = 1.7\Lambda > \mu^2_{\rm crit}$, $g^2 = \frac{1}{4}$ and $1.9\sqrt{\Lambda} \leq \chi(0) \leq 5.7\sqrt{\Lambda} \simeq \chi(0)_{\rm crit}$. Notice that we have here both positive and negative running $dn_s/d\ln k$ depending on the values of Λ and $\hat{\chi}(0)$. Most values of the running are negative in this regime. For $0.952 < n_s < 0.97$, we have $-0.001 < dn_s/d\ln k < 0$.

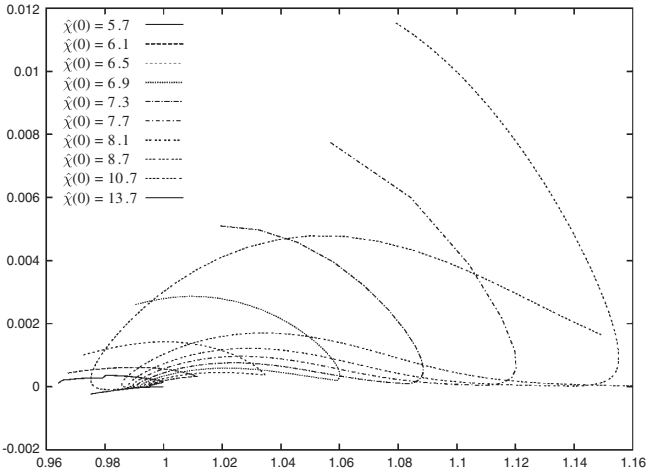

FIG. 23. Hybrid inflation. The running $dn_s/d\ln k$ vs n_s for $\mu^2 = 1.7\Lambda > \mu^2_{\rm crit}$, $g^2 = \frac{1}{4}$ and $\chi(0)_{\rm crit} \simeq 5.7\sqrt{\Lambda} \leq \chi(0) \leq 13.7\sqrt{\Lambda}$. Notice that we have here both positive and negative running $dn_s/d\ln k$ depending on the values of Λ and $\hat{\chi}(0)$.

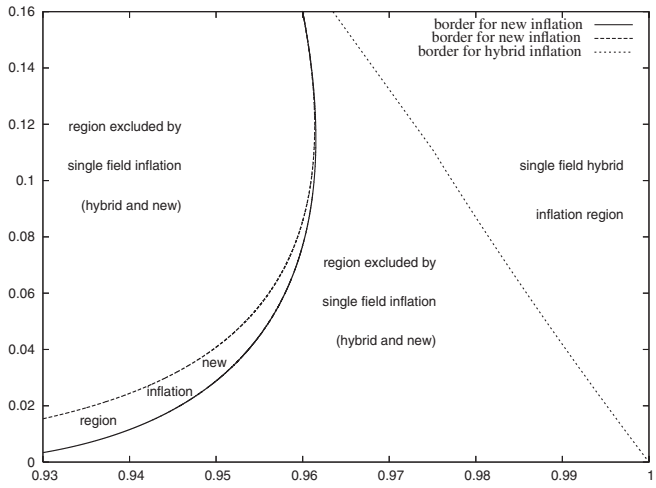

FIG. 24. Regions described in the (r, n_s)-plane by new and single-field hybrid inflation for $n_s < 1$. The hybrid inflation border corresponds to $\mu^2 = 1.7\Lambda$. For $n_s > 1$, all values of (r, n_s) can be described by hybrid inflation (at least for $r < 0.2$, $n_s < 1.15$). The excluded region cannot be described by single-field inflation (neither hybrid inflation, nor new inflation). Two or more fields inflation could describe such regions.

For $\hat{\chi}(0) > \hat{\chi}(0)_{\rm crit}$, all curves go towards $n_s = 1$, $r = 0$. Most of each curve lies in the $n_s > 1$ region, r monotonically decreases with n_s in the range $n_s < 1$ from the maximum $r_{\rm max}$ going towards $r = 0$ for $n_s \rightarrow 1$. For $\hat{\chi}(0) < \hat{\chi}(0)_{\rm crit}$ the curves pill up in the $n_s < 1$ region with almost the same slope, r sharply decreases in this region.

The curves for $\hat{\chi}(0) < \hat{\chi}(0)_{\rm crit}$ pill up in the $n_s < 1$ region with almost the same slope, r sharply decreases in this region.

All the blue tilted values of (n_s, r) in the domain $1 < n_s < 1.15, 0 < r < 0.2$ are realized by hybrid inflation.

The red tilted regime in hybrid inflation can only be realized for $\mu^2 > \mu^2_{\rm crit} \simeq 0.13\Lambda$. Moreover, the possible values of (n_s, r) are in the upper-right quadrant as shown in Fig. 24.

We see that hybrid inflation in the blue tilted regime $n_s > 1$ is strongly disfavored [Eq. (4.2)] [5]. That is, hybrid inflation in the regime $\hat{\mu}^2 < \hat{\mu}^2_{\rm crit}$ is strongly disfavored as well as hybrid inflation in the regime $\hat{\mu}^2 > \hat{\mu}^2_{\rm crit}$ with $\hat{\chi}(0) > \hat{\chi}(0)_{\rm crit}$.

Hybrid inflation in the red tilted regime $\hat{\mu}^2 > \hat{\mu}^2_{\rm crit}$ and $\hat{\chi}(0) < \hat{\chi}(0)_{\rm crit}$ fulfills the value for n_s Eq. (4.2), as well as the bound on the ratio r Eq. (4.3). We can read from Fig. 20 that

$$0.2 > r < 0.14 \quad \text{for } 0.952 < n_s < 0.97.$$

In addition, we find in Fig. 22 negative values for the running in this range, that is:

$$-0.001 < dn_s/d\ln k < 0 \quad \text{for } 0.952 < n_s < 0.97.$$

There are clearly two regions which are not covered by hybrid inflation with only one inflaton field, neither by new inflation as shown in Fig. 24.

Simple single-field inflation models have been recently studied within a numerical approach [15]. In ref. [16] cosmological data are fitted with the help of a Markov Chain Monte Carlo analysis.

There is an interplay between the bounds of neutrino masses and the sign of $(n_s - 1)$. A nonzero neutrino mass decreases the power in the small scales (large wavenumbers k). The same happens if n_s becomes smaller than unit. Therefore, *if* $n_s < 1$, the power spectrum permits more stringent tests of the neutrino masses [17]. The effect of neutrino masses for small scales $n_s > 1$ can be cancelled by a spectral index $n_s > 1$.

ACKNOWLEDGMENTS

We thank Daniel Boyanovsky for useful discussions.

[1] D. Kazanas, Astrophys. J. **241**, L59 (1980); A. Guth, Phys. Rev. D **23**, 347 (1981); K. Sato, Mon. Not. R. Astron. Soc. **195**, 467 (1981).

[2] V. F. Mukhanov and G. V. Chibisov, Pis'ma Zh. Eksp. Teor. Fiz. **33**, 549 (1981) [Sov. Phys. JETP Lett. **33**, 532 (1981)].S. W. Hawking, Phys. Lett. **115B**, 295 (1982); A. H. Guth and S. Y. Pi, Phys. Rev. Lett. **49**, 1110 (1982); A. A. Starobinsky, Phys. Lett. **117B**, 175 (1982); J. M. Bardeen, P. J. Steinhardt, and M. S. Turner, Phys. Rev. D **28**, 679 (1983); V. F. Mukhanov, H. A. Feldman, and R. H. Brandenberger, Phys. Rep. **215**, 203 (1992).

[3] P. Coles and F. Lucchin, *Cosmology* (John Wiley, Chichester, 1995); A. R. Liddle and D. H. Lyth, *Cosmological Inflation and Large Scale Structure* (Cambridge University Press, Cambridge, England, 2000); S. Dodelson, *Modern Cosmology* (Academic Press, New York, 2003); D. H. Lyth and A. Riotto, Phys. Rep. **314**, 1 (1999).

[4] C. L. Bennett *et al.* (WMAP Collaboration) Astrophys. J. Suppl. Ser. **148**, 1 (2003); A. Kogut *et al.* (WMAP Collaboration), Astrophys. J. Suppl. Ser. **148**, 161 (2003); D. N. Spergel *et al.* (WMAP Collaboration), Astrophys. J. Suppl. Ser. **148**, 175 (2003); H. V. Peiris *et al.* (WMAP Collaboration), Astrophys. J. Suppl. Ser. **148**, 213 (2003).

[5] D. N. Spergel *et al.* (WMAP Collaboration), astro-ph/

0603449; L. Page *et al.* (WMAP Collaboration), astro-ph/0603450; G. Hinshaw *et al.* (WMAP Collaboration), astro-ph/0603451; N. Jarosik *et al.* (WMAP Collaboration), astro-ph/0603452;

[6] D. Boyanovsky, H. J. de Vega, and N. G. Sánchez, Phys. Rev. D **73**, 023008 (2006).

[7] L. D. Landau and E. M. Lifshits, *Physique Statistique* (Mir Ellipses, Paris, 1994), Chap. 14; H. Leutwyler, Ann. Phys. (N.Y.) **235**, 165 (1994); S. Weinberg, hep-ph/9412326; *The Quantum Theory of Fields* (Cambridge University Press, Cambridge, 2000), Vol. 2.

[8] D. Cirigliano, H. J. de Vega, and N. G. Sanchez, Phys. Rev. D **71**, 103518 (2005).

[9] A. G. Sánchez *et al.*, Mon. Not. R. Astron. Soc. **366**, 189 (2006).

[10] U. Seljak *et al.*, Phys. Rev. D **71**, 103515 (2005).

[11] M. Tegmark *et al.*, Phys. Rev. D **69**, 103501 (2004).

[12] A. Linde, Phys. Rev. D **49**, 748 (1994); J. García Bellido and A. Linde, Phys. Rev. D **57**, 6075 (1998); E. J. Copeland, A. R. Liddle, D. H. Lyth, E. D. Stewart, and D. Wands, Phys. Rev. D **49**, 6410 (1994).

[13] A. R. Liddle, P. Parsons, and J. D. Barrow, Phys. Rev. D **50**, 7222 (1994).

[14] See, for example, W. Hu and S. Dodelson, Annu. Rev. Astron. Astrophys. **40**, 171 (2002); J. Lidsey, A. Liddle, E. Kolb, E. Copeland, T. Barreiro, and M. Abney, Rev. Mod. Phys. **69**, 373 (1997); W. Hu, astro-ph/0402060.

[15] L. A. Boyle, P. J. Steinhardt, and N. Turok, Phys. Rev. Lett. **96**, 111301 (2006).

[16] H. V. Peiris and R. Easther, J. Cosmol. Astropart. Phys. 07 (2006) 002.

[17] M. Fukugita, Nucl. Phys. B, Proc. Suppl. **155**, 10 (2006).